1968

Girder web boundary stresses and fatigue, WRC Bulletin No. 127, January 1968, Reprint No. 68-2

J. A. Mueller

B. T. Yen

LEHIGH UNIVERSITY INSTITUTE OF RESEARCH

Welded Plate Girders
- Design Recommendations

GIRDER WEB BOUNDARY STRESSES AND FATIGUE

by
J.A. Mueller
B.T. Yen

Fritz Engineering Laboratory Report No. 327.2

Progress Report on Welded Plate Girders

- Design Recommendations

GIRDER WEB BOUNDARY STRESSES AND FATIGUE

J. A. Mueller

B. T. Yen

Submitted to the

Welded Plate Girder Project Subcommittee

of the

Welding Research Council

Lehigh University
Department of Civil Engineering
Fritz Engineering Laboratory
Bethlehem, Pa.

July 1967

Fritz Engineering Laboratory Report No. 327.2

TABLE OF CONTENTS

ABSTRACT

The objective of this report is to define the primary cause of fatigue cracks observed in the webs of welded plate girder test specimens. The in-plane membrane stresses, which conformed reasonably well to beam theory predictions at the panel boundaries, are shown to have little connection with the occurrence of fatigue cracks, except in the tension region of panels under pure bending. The plate bending stress is then examined and a method of calculating these stresses through use of measured web deflections is developed. By taking into account the torsional rigidities of the flanges and transverse stiffeners, a partial differential equation is established as the necessary condition to ensure equilibrium and compatability between the web and its bounding elements. The subsequent solution of the equation is performed through the use of the finite difference technique. The accuracy of the resulting plate bending stresses is then examined. In comparison with stresses computed from measured strains, the method is proven reliable. It is shown that fatigue cracks always initiated at the points of maximum plate bending stress, that the sequence of crack formation on a single test girder is readily explained by these stresses and that a typical S-N distribution is obtained when the fatigue data of several girders are compared. It is concluded that the plate bending stress is a primary cause of fatigue cracks in thin-web welded plate girders.

1. INTRODUCTION

Prior to 1961, the design of plate girder webs was governed primarily by an elastic buckling criterion. Web slenderness ratios were restricted in order that web plates would not buckle. From a series of girder ultimate load tests,[1] it was shown that the elastic buckling loads could be exceeded in magnitude by several times. After methods of predicting girder carrying capacities were developed,[2,3,4] new design rules for buildings were prepared on the basis of a girder's ultimate strength which permitted the use of more slender webs.

Because design loads may now be greater than the web buckling loads, lateral web deflections of considerable magnitude can develop. This is illustrated in Fig. 1. When loads are less than the buckling value, the change in deflection is relatively small. However, if loads are substantially greater than the buckling value, deflections increase much more rapidly, often becoming several times the web thickness.

In order to evaluate the effect of these web deflections on the fatigue strength of girders, a number of investigations were undertaken on slender web girders.[5,6,7] It was found that webs deflected in specific patterns, depending on the loading condition. A summary of these patterns is given by representative contours of panels under bending, shear, and shear plus bending in Figs. 2, 3, and 4 respectively.[5] Initial web deflections are given in the upper portions of these figures, whereas deflections under load are below

them. From Fig. 2 it is seen that the bending panel contours retain their characteristically horizontal orientation even after load is applied. On the contrary, the contours of panels under shear become inclined in the direction of the panel tension diagonal as seen in Figs. 3 and 4. By comparing the deflections to the web thickness, it may be concluded that thin webs generally have initial deflections in the order of their thickness and that deflections under load increase to values that often may be twice the web thickness.[8]

When subjected to fatigue, webs will fluctuate between positions corresponding to the applied loads. Because of the large deflection magnitudes involved, investigators have observed fatigue cracks forming in locations characteristic of slender web girders.[5,6,7] From Fig. 5, the cracks are seen to occur along the compression flange or in the tension region along stiffeners of bending panels. Panels under shear were observed to incur fatigue cracks in the vicinity of the tension diagonal corners of the panel, as shown in the center portion of the figure. Cracks were also observed near the tension diagonal corners of the compression flange, and along the compression flange, for panels under shear and bending. In general, all cracks initiated in the web at the web toes of the panel fillet welds. They were normally first observed on one side of the web and usually propagated simultaneously through the web thickness and along the weld.

A specific cause of these fatigue cracks has not yet been completely correlated with experimental data. Inasmuch as the web deflections were large, they introduce membrane stresses and plate

bending stresses of unknown magnitudes along the panel boundary. Several investigators have discussed the relationship between web deflections and these plate stresses qualitatively.[9,10] Continuing in this vein, the purpose of this work is twofold: first, to quantitatively examine the plate membrane stresses and develop a method of calculating plate bending stresses along panel boundaries; and second, to investigate the correlation between boundary stresses and observed fatigue cracks. Membrane stresses will be studied first, followed by a study of the plate bending stresses.

2. WEB MEMBRANE STRESSES

In fatigue studies, the state of stress at the point where a crack initiates is the most important quantity with which fatigue life is correlated. Since most cracks considered in this investigation (Fig. 5) appeared first at the surface of the web, the surface stresses at the crack locations must be examined.

Any point on the web surface is subjected to the combination of membrane and bending stresses as shown in Fig. 6. The membrane stresses are constant in magnitude across the web thickness, whereas the bending stresses linearly vary from zero at the center of the web thickness to a maximum on the surface. Hereafter, membrane and bending stresses are denoted as such by subscripts m and b, respectively.

Although many investigators have examined weldments similar to those along flanges and stiffners of girder webs when subjected to normal membrane stresses,[11] little work has been devoted to the combined state of stress where membrane and bending stresses exist. The object of this chapter is to study the correlation between fatigue cracks and girder membrane stresses alone so as to determine whether it is necessary to correlate cracks with plate bending stresses. Because of the crack locations, only the membrane stresses along panel boundaries will be reviewed.

2.1 Web Boundary Membrane Stresses and Beam Theory Predictions

Shearing and normal membrane stresses in any flexural member may be compared with those predicted by ordinary beam theory. The orientation of the stresses from beam theory is shown in Fig. 7 for points near a stiffener or flange. Inasmuch as the web of slender girders deflects laterally and causes changes in the membrane stresses at its boundaries, the stresses predicted by beam theory could be modified. The extent of the modification was experimentally studied[5] and selective results are presented in Figs. 8, 9, and 10.

Normal membrane stresses in the longitudinal direction (σ_{mx}) agree well with the beam theory predictions for panels under pure bending, shear, and shear plus bending as seen in Figs. 8a, 9a, and 10a for loads up to 65% of the load-carrying capacity of a panel (P_u). It was also found that normal stresses perpendicular to the flanges (σ_{my}) were always small. In the bending panels, this stress was practically zero. This is shown in Fig. 8b where it is noted that $\epsilon_{my} = -\mu \cdot \epsilon_{mx}$, the required elasticity relation for $\sigma_{my} = 0$. Normal stresses parallel to stiffeners (σ_{my}) were always compressive, never amounting to more than -5 ksi. Both of these vertical normal stresses will be considered negligible in future calculations.

Shearing membrane stresses are compared with beam theory values in Figs. 9b and 10b. For the panels under shear, the experimental values were again in reasonable agreement (Fig. 9b) up until 0.65 P_u. In Fig. 10b, however, it is seen that the shearing stress departs appreciably from the beam theory predictions for the panels under

combined shear and bending, especially along the flanges, becoming larger in the vicinity of the tension diagonal corners and decreasing near the other corners. By comparing this figure with Fig. 5, it may be observed that the maximum shearing stress occurs in locations where fatigue cracks often developed.

From the good agreement between experimental data and beam theory values, it is concluded that the lateral web deflections do not cause marked deviations from beam theory predictions along the web boundary. In this report, then, beam theory stresses will be used to represent boundary stresses in correlation with crack data, with the lone exception of the shearing stresses along flanges where measured data will be used.

2.2 Web Membrane Stresses and Fatigue Life

Using the beam theory stresses and data from Ref. 5, normal stresses were computed for points on the web at which cracks were first observed. These stresses were then compared to the number of cycles at which the corresponding cracks formed. Two cases may be distinguished: welds along stiffeners which extend in a direction perpendicular to the applied normal stress and flange fillets which are parallel to the normal stress.

First, the results along stiffners are presented in Fig. 11. The sketch in the figure shows the web stiffener detail and the connecting fillet welds together with the direction of the applied stress (σ_{mx}) which is either tensile or compressive. The ordinate in the

plot is the range of the normal stress where the range is defined as the difference in the stresses corresponding to the maximum and minimum loads. Although the maximum and minimum stresses are usually specified to define the fatigue loading,[12] investigators have found that the range of stress has yielded consistent results for fillet welded joints. This has been observed to be true over a wide range of values of the ratio of the minimum to maximum stress for both non-load-carrying[13] and load-carrying[14] fillet welds. For this study, whenever stress is compared to fatigue life, the range of stress will be used.

Based upon Fig. 11, a wide scatter in test results is noted. Except for the three points in the upper portion of the figure, all stresses are less than 9 ksi. Since the range of stress required to cause fatigue cracks in this type of detail at 2,000,000 cycles has always been observed to be no less than about 14 ksi[15] and often as high as 20 ksi,[11] it is concluded that the normal stress did not cause those fatigue cracks with stresses less than 9 ksi. The three highest points plotted in Fig. 11 correspond to cracks in the web near a tension flange of a bending panel where all but the Mc/I stresses were negligible. Thus, although the membrane normal stress was of a sufficiently high magnitude to cause cracks similar to those shown along the right stiffener of the bending panel of Fig. 5, it does not give any consistent correlation for the other stiffener cracks shown in Fig. 5.

The normal stress is next compared to fatigue life in Fig. 12 for cracks located along the flanges. The sketch of the joint shows the orientation of web and flange and the direction of the applied

stress. As with the previous case, there is no consistency between the normal stress and the fatigue life. For example, at about 340,000 cycles stresses of 1 ksi are as likely to cause cracks as stresses of 12 ksi.

From these comparisons, then, it is concluded that the normal membrane stress alone can not generally explain the fatigue results obtained.

Next, the shearing membrane stress is compared with fatigue life in Fig. 13 because fatigue cracks and maximum shearing stresses occurred near the tension diagonal corners of a panel. Again, the plot is not completely conclusive. For example, cracks form as readily at 400,000 cycles as at 2,000,000 cycles for a shearing stress range of about 8.5 ksi.

Finally, other investigators have found that the maximum principal stress can give good correlation with fatigue life when both shearing and normal stresses are present at a point of crack initiation.[11] In Fig. 14 the principal tensile stress at crack locations is compared with the corresponding number of cycles to the cracks. The beam theory values were used in all cases since only minor deviations from experimentally measured values exist.[5] The test points again are distributed uniformly throughout the plot and indicate that the principal stress does not correlate at all with the fatigue life.

On the basis of the experimental data reviewed in this chapter, it is concluded that neither the normal nor shearing membrane stress,

nor their combination in the form of principal stress, provides any correlation with the observed fatigue lives of corresponding cracks.

Consequently, in the next chapters, the other surface component of stress - the plate bending stress - will be studied in an attempt to explain the fatigue results.

3. DETERMINATION OF WEB PLATE BENDING STRESSES

Investigators have reported surface stresses along girder web boundaries which are greatly different than those predicted by beam theory.[5,6] Since the membrane components of these stresses do not differ much from those by beam theory, and do not correlate well with fatigue behavior, plate bending stresses of considerable magnitude must exist which might explain the fatigue cracks observed.

Three panels of test girders[5] are presented with their measured plate bending stresses in Fig. 15. In the figure, the vectors represent plate bending stresses on the surface of the web facing the reader. Vectors acting away from the boundary are tensile, the others are compressive. All stresses less than 2 ksi are shown by the solid dots. For the bending panel, stresses are highest along the compression flange and are negligible in the tension region. Cracks parallel to the compression flange of the bending panel, shown in Fig. 5, could very well be related to this plate bending stress. The shear panel of Fig. 15, and the panel under shear plus bending, show that the plate bending stresses are highest near the tension diagonal corners, exactly where most of the cracks occurred for these loading conditions. The plate bending stresses are large in magnitude, reaching 36 ksi along the top flange of the shear and bending panel of Fig. 15.

In order to analyze the cracks with respect to the plate bending stresses, the distribution of these stresses must be known along

the web boundary. If a theoretical approach is to be taken, these stresses are obtained by satisfying the equations of large deflection theory.[16,17] These governing equations are a set of coupled, partial differential equations of the fourth order for which, in the general case, closed solutions are non-existent. Several investigators have solved particular cases of loading and boundary conditions and a comprehensive bibliography of work in this field has been compiled.[18] In most solutions, plate boundaries were either simply supported or fixed; in the limited cases of elastically supported edges the interest has been largely confined to the buckling problem.[19]

Although it is possible to predict the lateral web deflections under load from the initial web deflections, the purpose of this paper is to evaluate the plate bending stresses along panel boundaries and correlate these stresses with fatigue behavior. Inasmuch as changes in the lateral web deflections are known, the plate bending stresses may be obtained directly from these measured lateral deflections. Therefore, a semi-empirical method, using measured web deflections, will be developed to evaluate plate bending stresses along web boundaries. The analysis will be presented for the stiffener-web junction and any modifications required for the flange-web joint will be noted.

3.1 Plate Bending Stresses from Web Deflections

As a web deflects laterally, it tends to rotate the flanges or stiffeners to which it is rigidly attached. Since the flanges and stiffeners possess torsional rigidity, they resist this movement and

plate bending stresses are generated in the web. The solution of the plate bending stresses is, then, dependent on satisfying equilibrium and compatibility conditions at the boundaries.

The necessary conditions for the formulation of equilibrium and compatibility are sketched in Fig. 16 for the stiffener joint. In the upper portion of the figure, panel outlines are shown with the coordinate system and orientation of a differential element upon which equilibrium is to be enforced. If plate bending moments to the left and to the right of the stiffener centerline in the differential element are designated by $M_{x\ell}$ and M_{xr} respectively, then, for equilibrium:

$$m_t = M_{xr} - M_{x\ell} \tag{3.1}$$

where m_t is the distributed twisting moment in the stiffener. The positive directions of the moments are shown vectorially in the center part of Fig. 16.

By assuming that the angle between the stiffener and the web remains the same before and after loading, the required compatibility condition is:

$$\theta = - \partial w/\partial x \tag{3.2}$$

where θ is the angle of twist of the stiffener, shown positive in the lower portion of the figure, and w is the change in the lateral web deflection caused by external loads.

For the stiffener, considered now as a torsion bar subjected to distributed twist, m_t, the relationship between the twisting moment

and the angle of twist is:[20]

$$m_t = I_\omega \cdot \partial^4\theta/\partial y^4 - GK_t \cdot \partial^2\theta/\partial y^2 \qquad (3.3)$$

where I_ω and GK_t are the warping and torsional rigidities. Since the stiffener consists of narrow rectangles, joined at a single point, the warping rigidity becomes negligible and Eq. 3.3 simplifies to:

$$m_t = - GK_t \cdot \partial^2\theta/\partial y^2 \qquad (3.4)$$

The torsional constant K_t of a stiffener with two equal plates may be computed from[21]

$$K_t = 2(b_s \cdot t_s^3/3) \qquad (3.5)$$

where b_s and t_s are the width and thickness of a single stiffener plate.

The plate bending moments of Eq. 3.1 are expressed as[22]

$$M_x = -D\ (\partial^2 w/\partial x^2 + \mu \cdot \partial^2 w/\partial y^2) \qquad (3.6)$$

where D is the plate flexural rigidity. Since the stiffener has more resistance to lateral movement than the web, it will be assumed to remain straight. Consequently, the curvature in the vertical direction along the stiffener is zero and Eq. 3.6 can be rewritten as:

$$M_x = -D \cdot \partial^2 w/\partial x^2 \qquad (3.7)$$

Substituting Eqs. 3.2, 3.4, and 3.7 into 3.1, the boundary condition at the stiffener becomes

$$GK_t \cdot \partial^3 w/\partial x \partial y^2 = -D \left[(\partial^2 w/\partial x^2)_r - (\partial^2 w/\partial x^2)_\ell \right] \qquad (3.8)$$

where the subscripts r and ℓ refer to the portion of the web to the right and left of the stiffener, respectively.

The semi-empirical method of evaluating the plate bending stresses along the stiffener, then, consists of ensuring that the measured lateral web deflections satisfy Eq. 3.8 at discrete points.

Instead of using continuous derivatives of the deflection, the finite difference method will be employed.[23] A square mesh will be used whose mesh spacing (λ) is equal to the web depth (b) divided by the desired number of mesh spaces (n). Equation 3.8 can then be written in difference form as:

$$\Delta_{xyy}w + k\left[(\Delta_{xx}w)_r - (\Delta_{xx}w)_\ell\right] = 0 \qquad (3.9)$$

where $k = 2D\lambda/GK_t$ and $\Delta_{xx}w$ and $\Delta_{xyy}w$ are the second and third central differences of deflection in the subscripted directions, evaluated at the stiffener. For point co on a stiffener, as indicated below, these differences are:

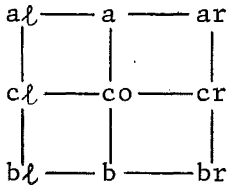

$$\Delta_{xx}w = w_{c\ell} - 2w_{co} + w_{cr} = w_{c\ell} + w_{cr} \qquad (3.10)$$

$$\Delta_{xyy}w = -w_{a\ell} + 2w_{c\ell} - w_{b\ell} + w_{ar} - 2w_{cr} + w_{br} \qquad (3.11)$$

where w_{co}, w_a, and w_b are equal to zero, since these points lie on the stiffener. For a panel to the left of the stiffener, w_{ar}, w_{cr}, and

w_{br} are unknown imaginary deflections, whereas for a panel to the right, $w_{a\ell}$, $w_{c\ell}$, and $w_{b\ell}$ are the unknowns.

By substituting Eq. 3.10 and 3.11 into Eq. 3.9, the boundary condition in terms of deflections is then:

$$(-w_{a\ell} + 2w_{c\ell} - w_{b\ell} + w_{ar} - 2w_{cr} + w_{br}) + k\left[(w_{c\ell} + w_{cr})_r - (w_{c\ell} + w_{cr})_\ell\right] = 0 \tag{3.12}$$

If Eq. 3.12 is written for each mesh point on the stiffener, a set of simultaneous equations for the unknown imaginary deflections results. After these imaginary deflections are solved, the curvature, and hence the stresses, may be determined at the mesh points along the stiffener.

Therefore, by using known deflections as input, the desired stresses along a stiffener may be obtained for one particular mesh spacing. Repeating the process for a different mesh spacing, stresses may be determined for the corresponding mesh points on the stiffener.

3.2 Extrapolation of Derivatives for Finite Difference Method

The central differences of Eqs. 3.10 and 3.11 are approximations of the corresponding derivatives. The magnitude of error involved depends on the mesh spacing chosen, being larger for the coarser grids and decreasing with smaller mesh spacings. It has been shown that, for central differences, the error caused by the approximation for any derivatives, or partial derivative, is proportional to the square of the

mesh spacing if the spacing is small enough.[24] This is shown below for the second derivative at a point on the web.

In Fig. 17a, the web deflection along a horizontal line is represented by the solid curve. Deflections $w_{c\ell}$, w_{co}, and w_{cr} are shown at equally spaced distances (λ) along the x-axis. If the curve is represented by a polynomial[25]

$$w = a_o + a_1 x + a_2 x^2 + a_3 x^3 + a_4 x^4 + \ldots \qquad (3.13)$$

then the derivatives of w at point b are:

$$(dw/dx)_b = a_1, \quad (d^2w/dx^2)_b = 2 \cdot 1 \cdot a_2, \ldots \qquad (3.14)$$

That is, the coefficients of Eq. 3.13, with proper constants, are the derivatives of w at point co. By writing Eq. 3.13 for $x = -\lambda$, o, and λ and solving for a_2:

$$2\,a_2 = (d^2w/dx^2)_{co} = (w_{c\ell} - 2w_{co} + w_{cr})/\lambda^2 - 2\lambda^2 a_4 - 2\lambda^4 a_6 - \ldots$$

or

$$(d^2w/dx^2)_{co} = (\Delta_{xx}w)_{co}/\lambda^2 - 2(\lambda^2 a_4 - \lambda^4 a_6 - \ldots) \qquad (3.15)$$

Thus, the second derivative at point co is equal to the second difference at point co divided by λ^2 minus the error terms. As the mesh spacing decreases, the higher order error terms become negligible[24] and

$$(d^2w/dx^2)_{co} = (\Delta_{xx}w)_{co}/\lambda^2 - 2\lambda^2 a_4 \qquad (3.16)$$

Thus, the second derivative at a point is equal to the second difference minus the predominant error term, which is a function of λ^2. For

central differences, this same procedure could be applied to any derivative, or partial derivative, and the same result would be obtained, that is, that the error in a derivative at a point is a function of the square of the mesh spacing.

Referring to Eq. 3.16 again, two unknown derivatives are present; the second derivative expressed as d^2w/dx^2 and the fourth derivative indicated by a_4. Both derivatives are independent of the mesh spacing. Writing Eq. 3.16 for two different mesh spacings, λ_1 and λ_2, a_4 can be eliminated. The second derivative at a given point then becomes:

$$d^2w/dx^2 = \phi_1 - \frac{\phi_1 - \phi_2}{\lambda_1^2 - \lambda_2^2} \cdot \lambda_1^2 \qquad (3.17)$$

where $\phi_1 = \Delta_{xx}w/\lambda_1^2$. Equation 3.17 represents a straight line on a $\phi - \lambda^2$ coordinate system as shown in Fig. 17b. If then, the second differences are known at one particular point for two different mesh spacings, the derivative may be extrapolated to a reasonable degree of accuracy when the chosen mesh spacings are small enough.

The method of extrapolation for derivatives adopted in this paper is best explained by referring to Fig. 17c. Using the second derivative as an example again, values of ϕ were calculated for four different mesh spacings for a particular point along a stiffener and the results plotted with respect to λ^2. It was generally found that the points did not lie on a straight line but that the slopes between adjacent points differed slightly. This indicates that the mesh

spacings are not sufficiently small to allow linear extrapolation of the derivatives from two points. To account for these slight changes in slope, a parabola was passed through the $\emptyset$ values of the finer three mesh spacings, corresponding to points 2, 3, and 4 in the figure, and the derivative extrapolated from this curve. Then a second parabola was passed through points 1, 3, and 4 and another value for the derivative calculated. If the extrapolations differed greatly, it was concluded that the results were unreliable since the parabolas were not approaching a straight line. Only when the extrapolations were within a few percent of each other were results considered acceptable.

With the second derivatives of web deflection known through the above extrapolation procedure, the moments to the left and right of the stiffener ($M_{x\ell}$ and M_{xr}) can now be determined from Eq. 3.7. In the following sections, some details of computing the plate bending stresses for girder webs will be discussed.

3.3 Computation of Stresses Along Stiffeners

The finite difference method of computing stress along the stiffener of a girder web was carried out in five steps.

1. With web deflections known at certain points on a web, a double interpolation was made to calculate web deflections at mesh points.

In Fig. 18, the relative locations of the measured deflections are depicted in the upper left by the solid dots and the mesh point deflections are shown as triangles. First, polynomials were fitted to

measured deflections in vertical cross sections, section A-A, with the flanges considered fixed. Consequently,

$$w_v = c_1 + c_2 y + \ldots . c_{m+4} y^{m+3} \qquad (3.18)$$

where m is the number of measured deflections. Deflections were then calculated at y - coordinates of mesh points (open circles in Fig. 18) and horizontal curves passed through these values. This is shown in section B-B where it will be noted that a point from a cross section in a neighboring panel has been included to approximate the slope of the curve at the stiffener. Thus,

$$w_h = c_1 x + c_2 x^2 + \ldots . c_n x^n \qquad (3.19)$$

for n number of cross sections. From Eq. 3.19 the mesh point deflections were subsequently obtained.

2. With deflections known for adjacent web panels, Eq. 3.12 was then written for each mesh point on the stiffener in order to evaluate required differences.

The arrangement and notation of deflections is shown in Fig. 19. Interpolated deflections are denoted by w_ℓ or w_r and imaginary deflections designated u_ℓ and u_r for the left and right panels, respectively. By using this notation, Eq. 3.12 becomes:

$$-w_{\ell-1} + 2w_\ell - w_{\ell+1} + u_{\ell-1} - 2u_\ell + u_{\ell+1}$$

$$+ k \left[w_r + u_r - (w_\ell + u_\ell) \right] = 0 \qquad (3.20)$$

Since the slope at the stiffener centerline is the same for the left and right panels,

$$(u_\ell - w_\ell)/2\lambda = (w_r - u_r)/2\lambda \qquad (3.21)$$

Solving for u_r from Eq. 3.21, substituting into Eq. 3.20 and rearranging:

$$u_{\ell-1} - 2u_\ell (1+k) + u_{\ell+1} = w_{\ell-1} - 2(w_\ell + kw_r) + w_{\ell+1} \qquad (3.22)$$

By writing this equation for each mesh point on the stiffener, a set of simultaneous equations was generated and the imaginary deflections were calculated. Then first and second differences were obtained at corresponding mesh points from the appropriate difference equations. The procedure was repeated until these differences were computed for all desired mesh spacings.

3. For each mesh spacing, polynomials were fitted through the calculated first and second differences and interpolations made for every twentieth point along the stiffener.

4. The values of the first and second derivatives at each twentieth point were then obtained from the extrapolation procedure outlined in Section 3.2.

An example of the method is given in Fig. 20 where the ordinate is the function $\emptyset$ and the abscissa is the square of the mesh spacing. The most satisfactory results were obtained for mesh spacings corresponding to dividing the panel depth of 50" into 14, 16, 18, and 20

equal parts. Parabolas were passed through points 2, 3, and 4 and points 1, 3, and 4 and the second derivative extrapolated as 0.01138 and 0.01122 from the two curves. These values were within the desired accuracy and the value of 0.01138 was adopted as the value of the second derivative (curvature).

5. With the slope and curvature known at every twentieth point along the stiffener, the next step was to calculate the stresses at the toe of the weld and at strain gage locations. Coordinates and reference distances are shown in Fig. 21a for the web-to-stiffener joint, whereas, in Fig. 21b, the web is shown after load was applied. To represent the elastic curve of the plate a polynomial was assumed:

$$w = c_1x + c_2x^2 + c_3x^3 + c_4x^4 + c_5x^5 \qquad (3.23)$$

By substituting three deflection conditions and enforcing the slope and curvature conditions at the center of the stiffener, the coefficients of the equation were determined.

Assuming the stiffener to remain laterally undeflected, the stress at the toe of the weld is then computed from Eq. 3.23:

$$\sigma_{bx} = \frac{-E \cdot t_w/2}{1-\mu^2} \cdot \left.\frac{d^2w}{dx^2}\right|_{x_1} \qquad (3.24)$$

The gage stress was calculated from an average curvature over the gage length,

$$\sigma_{gage} = \frac{-E \cdot t_w/2}{1 - \mu^2} \cdot \frac{\int_{x_2}^{x_3} (d^2w/dx^2)dx}{x_3 - x_2} \qquad (3.25)$$

The assumption that the stiffener remains straight can be verified by comparing experimental plate bending stresses in the x and y-directions. In Fig. 22a these stresses (σ_{bx} and σ_{by}) are plotted versus load. Also indicated by the dashed line is the product of Poisson's ratio and σ_{bx}. It is seen that the curves for σ_{by} and $\mu\sigma_{bx}$ are almost coincident. From elasticity relations, this implies that the bending strain in the y-direction is zero. Consequently, the curvature parallel to a stiffener is negligible and stresses may be computed from the curvature in the x-direction alone. Similarly, the stresses along a flange may be computed from curvature in the y-direction (Fig. 22b).

The stresses obtained through application of steps 1 through 5 will be referred to as the results of the "first plate analysis" in subsequent discussions. To refine these values, the first and second derivative calculated in step 4 were incorporated in the horizontal interpolation curves (w_h) of the first step. Improved values of the mesh point deflections were then computed and steps 2 through 5 were repeated. The stresses from this second round of computation will be termed the results of the "refined plate analysis".

3.4 Computation of Stresses Along Flanges

The general procedure outlined for a stiffener was used to compute stresses along a flange. Using the coordinates and sign convention of Fig. 16, the basic equilibrium equation, Eq. 3.9 is then modified to:

For top flange: $m_t = M_y$ and $\theta = \partial w/\partial y$,

$$\Delta_{yxx}w - k\,(\Delta_{yy}w) = 0 \qquad (3.26)$$

For bottom flange: $m_t = -M_y$ and $\theta = +\partial w/\partial y$,

$$\Delta_{yxx}w + k\,(\Delta_{yy}w) = 0 \qquad (3.27)$$

In addition to these changes, the interpolation of deflections in the first step was carried out by passing horizontal curves from stiffener to stiffener. Then vertical curves were passed through the first interpolated deflections and a zero slope condition enforced at the flange. After the slope and curvature of the web were known along the flange, refined values of deflection and subsequent stresses were obtained.

Since the flanges were relatively rigid when compared to the web, flange rotations were generally quite small. By considering the flange fixed with respect to the web, an upper bound on the flange stress could be obtained which would be reasonably close to the value calculated from the method outlined above. In this procedure, then,

vertical curves were passed through three measured deflections adjacent to the flange, as shown in Fig. 23, where

$$w_c = c_1 y^2 + c_2 y^3 + c_3 y^4 \qquad (3.28)$$

Toe and gage stresses were then computed by substituting the derivatives of Eq. 3.28 into Eqs. 3.24 and 3.25.

4. RESULTS OF PLATE BENDING STRESS ANALYSIS

The method of plate bending stress analysis described in the last chapter was applied to several test girders from Ref. 5. The stresses so obtained are presented and discussed here for web panels under shear, bending, and their combination to verify the method's general applicability.

4.1 Plate Bending Stresses Normal to Stiffeners

First, the computed plate bending stresses (σ_{bx}) along vertical lines at which gages were located were compared with the stresses obtained from the measured gage strains. These calculated and "measured" stresses are shown in Fig. 24 for the three loading conditions. All stresses shown are on the positive z-surface of the web and are tensile if plotted in the direction of the positive σ_{bx} axis. The results of the first plate analysis are shown in dashed lines on the same cross sections as those of the refined plate analysis which are indicated by the solid lines. The magnitudes of the stresses from measurements (dots) are also superimposed at their proper locations. Regardless of the loading condition, the stresses resulting from both the first and the refined plate analysis correlate well with the measured values. This agreement is particularly good between the stresses from the refined plate analysis and the measured data.

Next, the plate bending stresses at the web toes of the fillet welds are examined with the aid of Fig. 25. Both the results of the first and the refined plate analyses are presented. For all three loading conditions, the magnitudes of stress obtained through the refined analysis are expectedly lower than those from the first plate analysis by a small amount. In the cases presented, the maximum value of refinement is about 20%. It is concluded that, although the gage stresses from both analysis are almost the same, the refinement is required to establish reliable toe stresses.

For the shear panel of Fig. 25, the toe stress is seen to exceed the yield stress of the web (σ_y) by a slight amount. However, since the yield stress was determined by a standard tensile test, it does not include any lateral stresses. If von Mises' yield criterion is adopted, it can be shown that the web stress may exceed the simple tensile test yield stress by a maximum of 15% when stresses parallel to the boundary are present. Even though this increase in yield stress may not always account for the difference between the maximum computed stress and the linear yield stress, yielding over a limited length of a boundary will be considered a localized effect which does not detract from the validity of the results.

For both the gage stresses and the stresses at the toes of the welds the results presented are too limited to indicate any pattern of stress distribution. However, in comparing the stresses along corresponding vertical sections, Figs. 24 and 25, it is obvious that the distribution of plate bending stresses at the toes of the welds is the

same as that along the vertical gage line nearby. For all three loading conditions the gage stresses are lower in magnitude. This is because plate bending stresses are of a localized nature and decrease rapidly away from the stiffener. The most pronounced difference is for the upper left panel in which the gages were mounted relatively far away (8 times t_w) from the web boundary than those of the other two panels (4 times t_w). Consequently, it can be concluded that gages must be mounted as close to the weld toe as possible so as to give a better indication of the plate bending stresses there. In any event, the stresses at toes of the welds are higher than those at the gages. Therefore, the gage stress provides a lower bound on the stress at the web toe of the fillet weld.

Before leaving the topic of stiffener stresses, it is proper to discuss a basic assumption used in deriving the boundary stresses - that the bending rigidity of the web is constant between the center-lines of the stiffeners of a panel. This condition is depicted in Fig. 26 as "model (a)". If the stiffener plates and the fillet welds are sufficiently large, the web between the toes of the fillets on either side of the stiffener becomes relatively rigid and may remain straight after loading, as shown in "model (b)". To compare the effects of these two extreme conditions, analyses were made using both assumptions and the resulting stresses calculated at gage locations are sketched in the lower portion of the figure for both sides of one stiffener. It is seen that the two models give the same distribution pattern of stresses, but different magnitudes, over a considerable length of the stiffener.

Results from model (b) are generally higher than those from model (a) for the cases presented. However, in comparing both with the measured gage stresses, model (a) seems to offer a better approximation.

Continuing this examination, the variation in the plate bending stresses in the local area of the fillet welds is presented next for the two models. In Fig. 27 an outline of a stiffener-to-web joint is shown in the upper part. Below, a plot of plate bending stress versus the distance in the x-direction is presented for the two web-to-stiffener models for point A of Fig. 26. Stresses of model (a) are greatest at the toe of the weld and decrease away from the stiffener. On the other hand, stresses of model (b) are smallest at the toe of the weld, increase as distance increases until a peak is reached, then begin to decrease. Because of the physical nature of the problem, resisting moments must be a maximum where restraint is introduced, that is, at the web-to-stiffener (or flange) intersection. Web stress will be greatest at the web toes of the fillet welds and decrease as distance from the restraints increase. The behavior of the plate bending stresses from model (b) at point A contradicts this condition and must be deemed unacceptable.

In order to generalize on this conclusion, the gage and toe stresses from models (a) and (b) are compared over the entire depth of the stiffener in Fig. 28. Stresses from model (b) are plotted in the upper portion of the figure for locations to the left and right of the stiffener which corresponds to that in Fig. 26. The gage stresses (dashed lines) exceed the stresses at the web toes of the fillet welds

over the total web depth, contrary to the results of model (a) in the lower part of the figure. This indicates that the unacceptable nature of model (b) is not limited to a single point, but to the entire panel boundary. Consequently, model (a) is used in all calculations of stresses along the stiffener and also along the flange.

4.2 Plate Bending Stresses Normal to Flanges

Computed and measured plate bending stresses at gage locations along the flanges are presented in Fig. 29 for the three loading conditions. The direction of the stress is perpendicular to the flange and is designated by σ_{by}. In all cases, either the results of the first plate analysis coincides with the refined analysis or very little difference exists between the two. For all loading conditions, good agreement exists between the calculated and measured stresses.

From the good agreement between the measured and calculated plate bending stresses along both stiffeners and flanges, it is concluded that the method of computing plate bending stress is reliable.

By using this method the toe stresses corresponding to the gage stresses of Fig. 29 are computed and plotted in Fig. 30. The results of the first and refined analyses are so close that the differences cannot be indicated in the figure. It appears as if the refinement is not required for flanges. This is explained by the fact that the torsional rigidity of the flange is quite high compared with that of a stiffener, resulting in flange rotations much smaller than those of the stiffener. Thus, corrections to the original interpolated

deflections are small and the refined analysis shows little difference from the first analysis.

Since the flange rigidity is high, it would be interesting to compare the results of the plate analysis and of the cantilever strip analysis described at the end of section 3.4. Thus, the stresses at the web toes of the fillet welds calculated by the cantilever model are also given in Fig. 30. It is clear from the curves that the cantilever strip approximation gives a stress distribution at the toe of the weld similar to that of the plate analysis. In neglecting the rotation of the flanges, the approximate method results in stresses slightly higher in magnitude than those from the more complicated method. The greatest difference in magnitude for the cases presented occurs in the bending panel which has relatively the least rigid flange of all three panels.

In order to look further into the possibility of using the cantilever strip analysis for a reasonable upper bound of plate bending stresses perpendicular to the flanges, an examination of the flange rigidity is in order. One measure of the relative flange rigidity is given by a ratio between the flange St. Venant torsional rigidity (GK_t) and the product of the plate bending stiffness and the panel length ($D \cdot a$).

With

$$GK_t = (E/2\ (1 + \mu)) \cdot (b_f \cdot t_f^3/3)$$

and

$$D = E\ t_w^3/12\ (1 - \mu^2),$$

then

$$GK_t/D \cdot a = 2 (1 - \mu)(b_f/a) \cdot (t_f/t_w)^3 \qquad (4.1)$$

Since Poisson's ratio is the same for all girders investigated, the relative flange rigidity is expressed as:

$$k_1 = (b_f/a) \cdot (t_f/t_w)^3 \qquad (4.2)$$

As the value of k_1 increases, the flange torsional rigidity gets larger and flange rotations decrease. Consequently, with higher values of k_1, the flange approaches the fixed-end condition and agreement between the cantilever strip analysis and the plate analysis improves. Therefore, the bending panel with $k_1 = 10$ has the relatively highest difference between the two methods, whereas the shear panel shows the best agreement since $k_1 = 48$. It is concluded that, given a sufficiently high value of k_1, the cantilever strip analysis can yield an upper bound on the plate bending stress reasonably close to the stresses from plate analysis.

In comparing Figs. 29 and 30, the shapes of the curves for the gage and toe stresses are quite alike and the magnitudes are in good agreement. For these three plots, the greatest difference between the maximum gage and toe stress is only about 15% of the toe stress for the shear panel which had gages mounted at a distance from the flange twice that of the other girders. Thus, as compared to the stresses along stiffeners, the flange plate bending stresses have a smoother gradient and diminish more slowly away from the flange. As with the stiffeners, the gage stresses are consistently lower than the toe stresses, once again providing a lower bound.

4.3 Web Deflections and Results of Plate Analysis

In order to show the overall relationship between the web deflections and the plate rotations and bending stresses, web deflection contours are plotted in Fig. 31 for two adjacent panels of a girder. The solid contour lines represent deflections out of the plane of the figure. Tensile stresses on the web surface facing the reader are designated positive. The sense of the boundary rotations are obtained from the right-hand rule.

First, the rotations are examined. For example, for the left panel, the negative web deflections in the upper right portion of the web rotate the top flange and the stiffener in corresponding directions, being positive for the flange and negative for the stiffener. The maximum values of the rotations at all boundaries agree with the location of the contours. It may be observed that the flange rotations are much smaller than those of the less rigid stiffener, being in the order of ten times less.

As with the rotations, plate bending stresses agree well with the web deflections. When deflections are positive, compressive stresses develop on the web surface facing the reader, as seen along the flange in the upper left portion of the left panel. Just to the right, where deflections are negative, tensile stresses are generated. By comparing the maximum stresses along the top flange of the left panel, the tensile stresses are larger in magnitude than the adjacent compressive stress. This follows since the negative deflections indicate a higher contour gradient than the nearby positive deflections.

Thus, from the agreement between the computed and measured stresses at gage locations along the entire panel boundary, and from the agreement between the web deflections and the calculated rotations and stresses, it is concluded that a reliable method of predicting plate bending stresses has been developed. The final step, a comparison of stresses and fatigue cracks, follows in the next chapter.

5. PLATE BENDING STRESSES AND FATIGUE

In the preceding chapters it was shown that the membrane stresses did not correlate well with observed fatigue behavior. Then, a method of computing plate bending stresses from measured web deflections was developed and verified. In this chapter, the calculated plate bending stress will be compared with fatigue results to show that these stresses are a primary cause of fatigue cracks in thin-web plate girders.

5.1 Locations of Cracks When First Observed

Along all web boundaries of girders investigated,[5] the cracks, when first observed, occurred in regions where the plate bending stresses computed according to the method developed in Chapter 3 were at their maximum values.

The plate bending stress along stiffeners is shown in Fig. 32. Superimposed on these plots are the locations of the cracks along the web toe of the web-to-stiffener fillet welds. All crack lengths are as first observed by investigators and were generally several inches long before being detected. Consequently, the points of initiation of the cracks must be within this length. In the following discussion, it will be assumed that the cracks initiated at the points within the initial lengths where the stress was highest.

By comparing the initial cracks to the plate bending stresses, it is seen that all cracks were located at points of maximum stress. Along each boundary, wherever the stress was highest, there the cracks occurred. Included in these plots is the upper right curve for a shear panel where the computed plate bending stress far exceeded the yield stress. Even in this case, the initial crack still occurs in the region of the maximum computed stress.

The same conclusions drawn above may be extended to the flange cracks when one considers Fig. 33. Along each flange-to-web intersection, the initial cracks were always located in the maximum bending stress regions. When two dominant maxima are present, such as the 25 and 38 ksi stresses of the bottom portion of the figure, cracks always occur at the absolute maximum -- at the 38 ksi location in this case.

In summarizing the fatigue cracks observed in thin-web girders (Fig. 5), it was pointed out that cracks usually occurred in particular locations according to the loading condition of a panel. For example, in panels under shear, cracks were confined to the vicinity of tension diagonal corners. This is explained by the fact that the maximum plate bending stress was located in those regions (Fig. 31).

As to the surface of the web on which cracks were first detected, the cracks generally occurred on that face which had tensile plate bending stresses. Out of twenty-one cracks, eighteen of them initiated on the web surface which was under tension from the plate bending stresses. One of the remaining cracks, which initiated on the compressive face, occurred in a region of severe local weld irregularities.

5.2 Sequence of Crack Formation

For test girders investigated, the sequence of crack formation correlated well with the magnitudes of plate bending stresses at the crack locations.

To examine this, plate bending stresses were determined along panel boundaries of a single girder and plotted in Fig. 34. A sketch of the girder specimen is shown in the upper portion of the figure. In the central and lower portions, using the panel outlines as a reference, initial plate bending stresses at the web toes of the fillet welds are plotted. Along stiffeners, stresses are given at the weld toe which had the highest maximum stress and are identified as to which panel they belong. The initial lengths of the cracks are also shown and are numbered in order of occurrence together with the number of cycles at which they were observed.

In chronoligical order, then, the first crack occurred in panel 5 at 350,000 cycles at a point where the highest girder stress of 38 ksi existed, whereas, crack 2 was observed at the same number of cycles in panel 6 at a stress of 32 ksi. Although a stress of 34 ksi is shown along the stiffener in panel 6, a crack did not occur there at 350,000 cycles. In part, this may have been due to a localized stress condition at the flange. Also, the small difference in stress level between the 32 and 34 ksi values is within the accuracy of the method of calculating these plate bending stresses. After cracks 1 and 2 had propagated several inches, they were repaired by welding and subsequently isolated by adding additional transverse stiffeners in panels 5 and 6.

Thereafter, the maximum plate bending stresses in these panels were reduced since the web deflections under subsequent loading were considerably smaller.

As fatigue loading was continued after the repair, the stresses of panels 2 and 3 were still at the values shown and crack 3 was observed along the stiffener of panel 3 after 650,000 cycles at 25 ksi. Without repairing this crack, fatigue loading was continued and crack 4 was detected at 860,000 cycles along the top flange of panel 2. It may be observed that the initial length of crack 4 did not correspond exactly with the location of the maximum plate bending stress. This crack was somewhat different than others. Initiating at a large weld discontinuity at 860,000 cycles, it did not propagate until 1,836,000 cycles contrary to the normal behavior of all other cracks. When it did propagate, its main direction of growth was toward the point of maximum bending stress.

A summary of the above information is listed below.

Crack	Plate Bending Stress (ksi)	N (cycles)
1	38	350,000
2	32	350,000
3	25	650,000
4	25	860,000

From the above, it is seen that the relationship between fatigue cracks and their occurrence is established through the plate bending stress. On the basis of the stress, a consistent explanation of the fatigue behavior results.

To examine the fatigue behavior of another girder, the plate bending stresses were calculated for a shear girder sketched in the upper portion of Fig. 35. This girder had no detectable cracks after 3,000,000 cycles of load. This phenomenon is explained when the calculated plate bending stresses are examined. It is seen that the bending stress never exceeded 21 ksi along the stiffeners and flanges. When compared with the stresses of Fig. 34, this magnitude is well below those causing the fatigue cracks of the preceding girder.

5.3 Plate Bending Stress and Fatigue Life

The plate bending stresses of several girders compare well with the numbers of cycles to cracks giving a typical S-N distribution.

The available data are presented in Fig. 36 where the range of the plate bending stress normal to the boundary along the crack is the ordinate and the number of cycles to the first observation of cracks is the abscissa. From this plot, it is seen that the plate bending stress alone provides a typical S-N distribution. Cracks along the flange are seen to be in the same range as the points representing cracks along the stiffeners, indicating the general correlation between the cracks and the plate bending stress.

From the plot a leveling off is beginning for a stress somewhere between 21 and 25 ksi. The two points with the arrows show that stresses of 21 ksi did not cause failure at 3,000,000 cycles. It appears, then, that an endurance limit lies between 21 and 25 ksi.

Since the cracks presented in Fig. 36 all formed on the web surface, a combination of the membrane and plate bending stresses in the form of the principal surface stress may yield even better fatigue correlation. A comparison of this stress with the number of cycles to cracks is given in Fig. 37 for the web surface on which the crack was first observed. The sketches in the lower left indicate the stress conditions at the flanges and stiffeners. For example, along the flange, the stress in the x-direction is a combination of the beam theory membrane stress and the bending stress due to the Poisson effect - as shown in Fig. 22. Perpendicular to the flange, only bending stresses are present. Shearing membrane stresses are also shown for both points.

From Fig. 37, it is seen that there is reasonably good correlation with the fatigue data. All values have been slightly increased above the stresses shown in the previous figure. Because there are no available S-N curves for the case of combined membrane and bending stress, it is difficult to decide whether the plate bending stress or the principal surface stress is the more significant. However, since the plate bending stress is the largest contributor to the principal stress, it is felt that it alone offers a significant S-N relationship.

Thus far, stress concentrations have not been considered in this paper. To be sure, all types of stress concentrations are present at the fillet welds along the web boundary. These include geometrical discontinuities such as caused by undercutting, weld convexity, and stop-start positions. The severity of the concentration in the elastic case is measured by the stress concentration factor (k_t) which is the

actual stress at the concentration divided by the nominal stress. As k_t increases, the actual stress increases and fatigue strength decreases. Taking the endurance limit as a reference, the loss in fatigue strength due to stress concentrations, or "notches", is defined by the fatigue reduction factor (k_f) where

$$k_f = \frac{\text{endurance limit of an unnotched specimen}}{\text{endurance limit of a notched specimen}}$$

Therefore, in the elastic case, as k_t increases, k_f increases.

Whenever yield strain has been reached in a material under fatigue loading, it has been found that the fatigue reduction factor begins to stabilize and becomes independent of the value of k_t. For plain carbon steel, k_f has been noted recently to be about 1.5 when plastic strains are encountered.[26] Since the stresses at the cracks indicated in Figs. 36 and 37 were well above the webs' yield points when stress concentrations and residual stresses are considered, computed values of k_f should be in the vicinity of 1.5.

Using the plate bending stress range as a reference, the endurance limit in the "notched" case is somewhere between 21 and 25 ksi (Fig. 36) whereas an endurance limit of from 24 to 27 ksi results if principal surface stress is used (Fig. 37). In both cases, the endurance limit in the "unnotched" condition is assumed as one-half the material's ultimate tensile strength.[11] From these values, k_f would vary from 1.1 to 1.7 and from 1.1 to 1.5 for the plate bending and principal stresses, respectively. It is seen that the ranges of

the k_f values for the girder test specimens are in the region of the independently observed values.

From the result that the plate bending stress correlates well with the locations of cracks, with the sequence of crack formation on a single specimen and with the S-N curve obtained from several specimens, it is concluded that this plate bending stress is the most significant factor causing the fatigue cracks in thin-web plate girders.

6. SUMMARY AND CONCLUSION

From the results of the investigation carried out in this paper on girder web bending stresses and fatigue, it has been found that:

1. Normal membrane stresses in the web conform well to beam theory predictions along the periphery of a panel. Shearing membrane stresses are also in agreement with beam theory along the stiffener boundaries. However, along the flanges, the shear stress exceeds the beam theory predictions near the tension diagonal corners and is less near the other corners.

2. Normal tensile membrane stresses may cause fatigue cracks in the tension region of panels subjected to pure bending. In all other loading cases, neigher the normal nor shearing membrane stress, nor their combination, appears to correlate at all with observed fatigue behavior.

3. A reliable method of calculating plate bending stresses at panel boundaries was developed. In this method, the torsional rigidity of the flanges and stiffeners was incorporated into a governing boundary condition which is in the form of a third order partial differential equation. By using measured web deflections, the boundary equation was solved numerically through a finite difference procedure. Stresses were calculated for mesh spacings corresponding to dividing the plate

dimension into 14, 16, 18, and 20 equal parts and extrapolating. These mesh spacings proved adequate for both the stiffeners and flanges.

4. The stresses calculated by the above method were in good agreement with stresses obtained from measured gage strains. This was true along stiffeners and flanges and for panels under shear, bending and shear plus bending. It was also shown that a cantilever strip could yield reasonably accurate values of plate bending stress normal to the flanges when the relative flange rigidity was sufficiently high.

5. Plate bending stresses normal to panel boundaries were shown to be the primary cause of the fatigue cracks. In all cases, cracks initiated at points of maximum plate bending stress along a single boundary. In considering the entire periphery of a single panel, a crack will initiate at the location where this stress is highest. When several panels of a single girder were compared, the sequence of crack formation corresponded well with the values of the plate bending stresses, with the higher stresses causing the first cracks. Finally, in comparing the plate bending stresses at crack locations of several girders, a typical S-N plot was generated.

In conclusion, the method developed in this paper may now be applied to plate girders with various geometrical and loading conditions to calculate the plate bending stresses along the web boundary. The stresses so generated can then be compared with the S-N curves of stiffener-to-web and flange-to-web weldments. Any computed stress which would cause fatigue cracks prior to a specified number of loading cycles

would not be permitted. Corresponding geometrical conditions would then be investigated to determine limiting values of the web slenderness and panel aspect ratios to be used in design recommendations. At present work is underway to evaluate the effect of various geometrical and loading conditions on the plate bending stresses on an analytical and experimental basis.

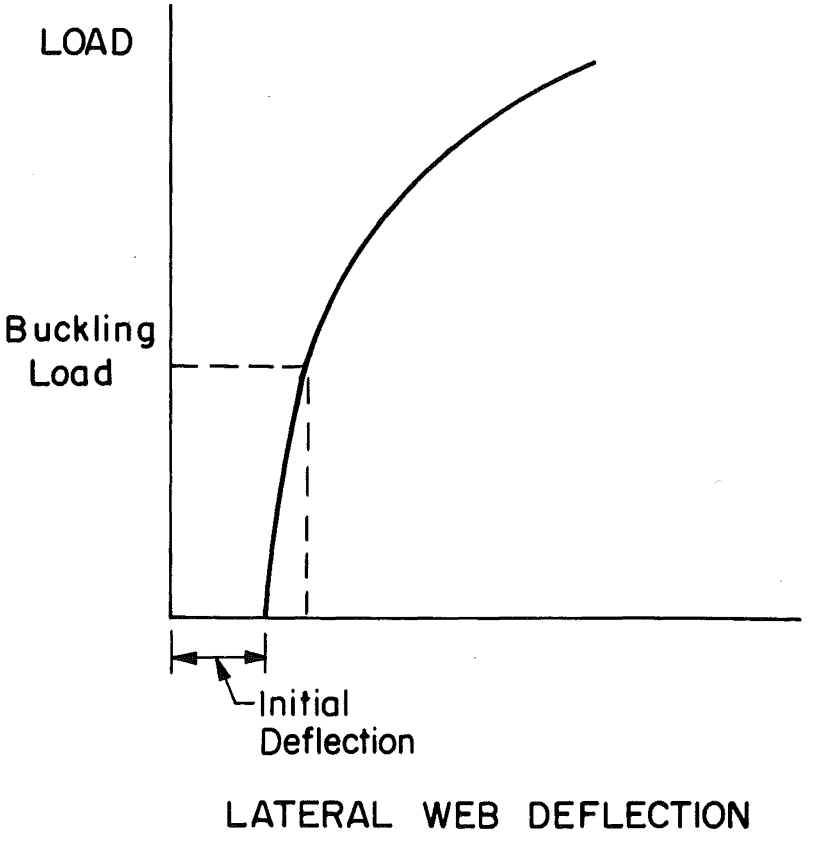

Fig. 1 Schematic Variation of Lateral Web Deflection Under Load

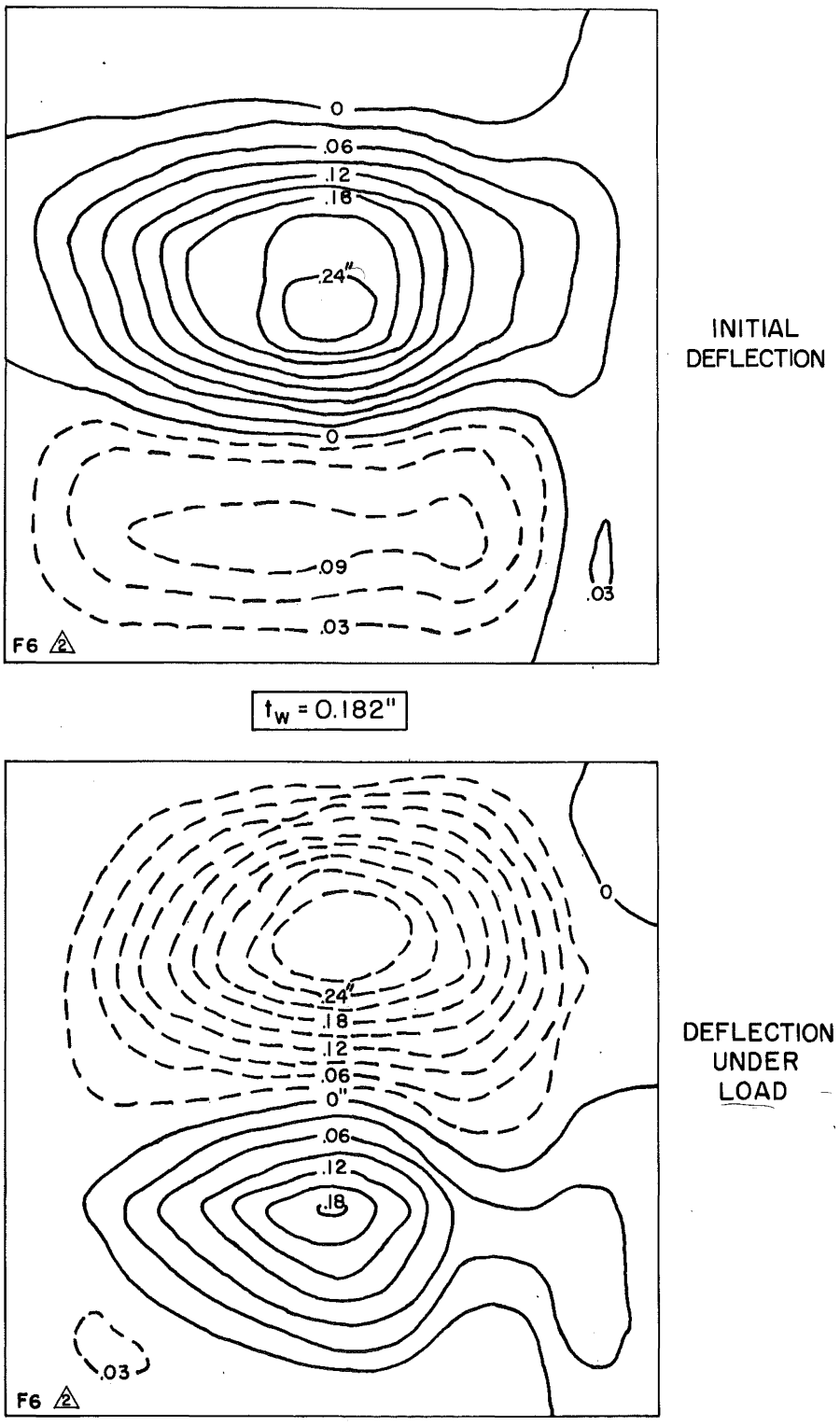

Fig. 2 Lateral Web Deflection Contours - Bending Panel

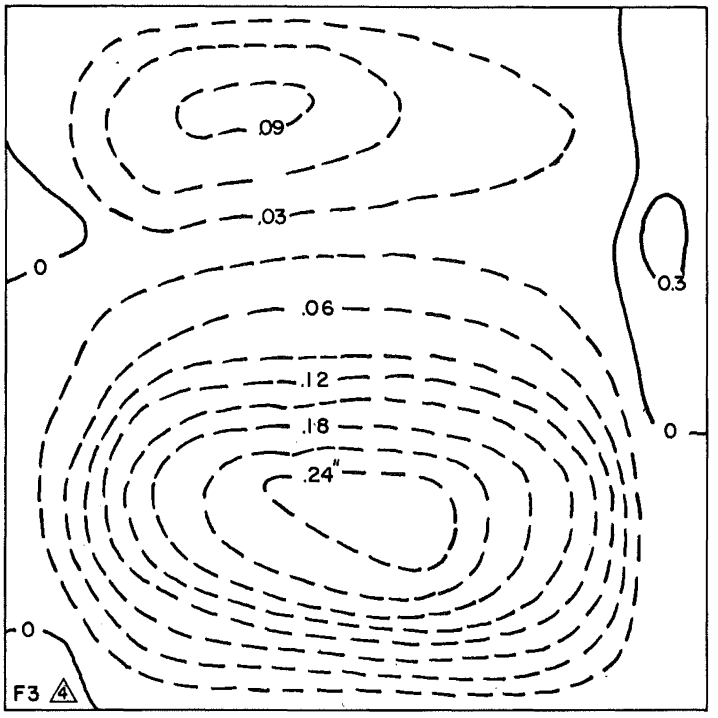

INITIAL DEFLECTION

$t_w = 0.174"$

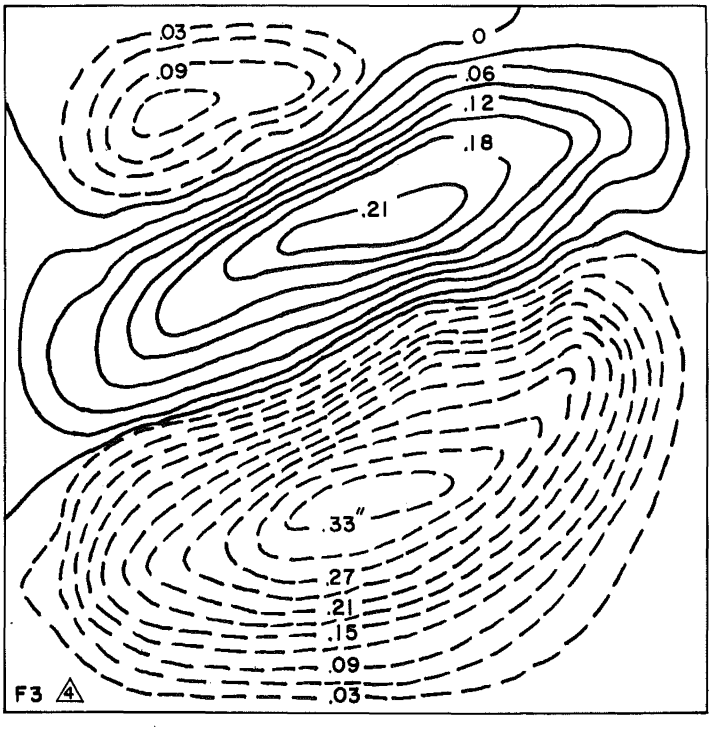

DEFLECTION UNDER LOAD

Fig. 3 Lateral Web Deflection Contours - Shear Panel

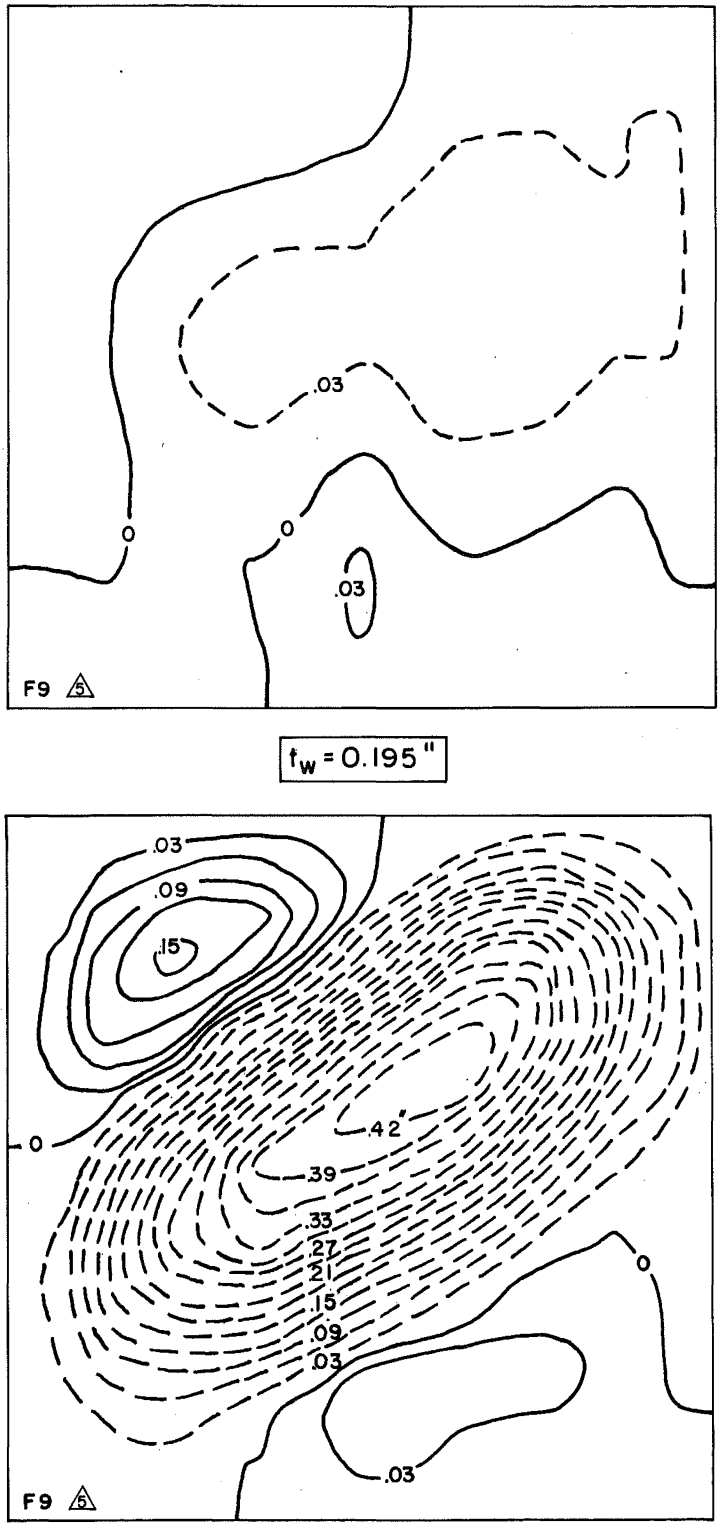

Fig. 4 Lateral Web Deflection Contours - Panel Under Bending and Shear

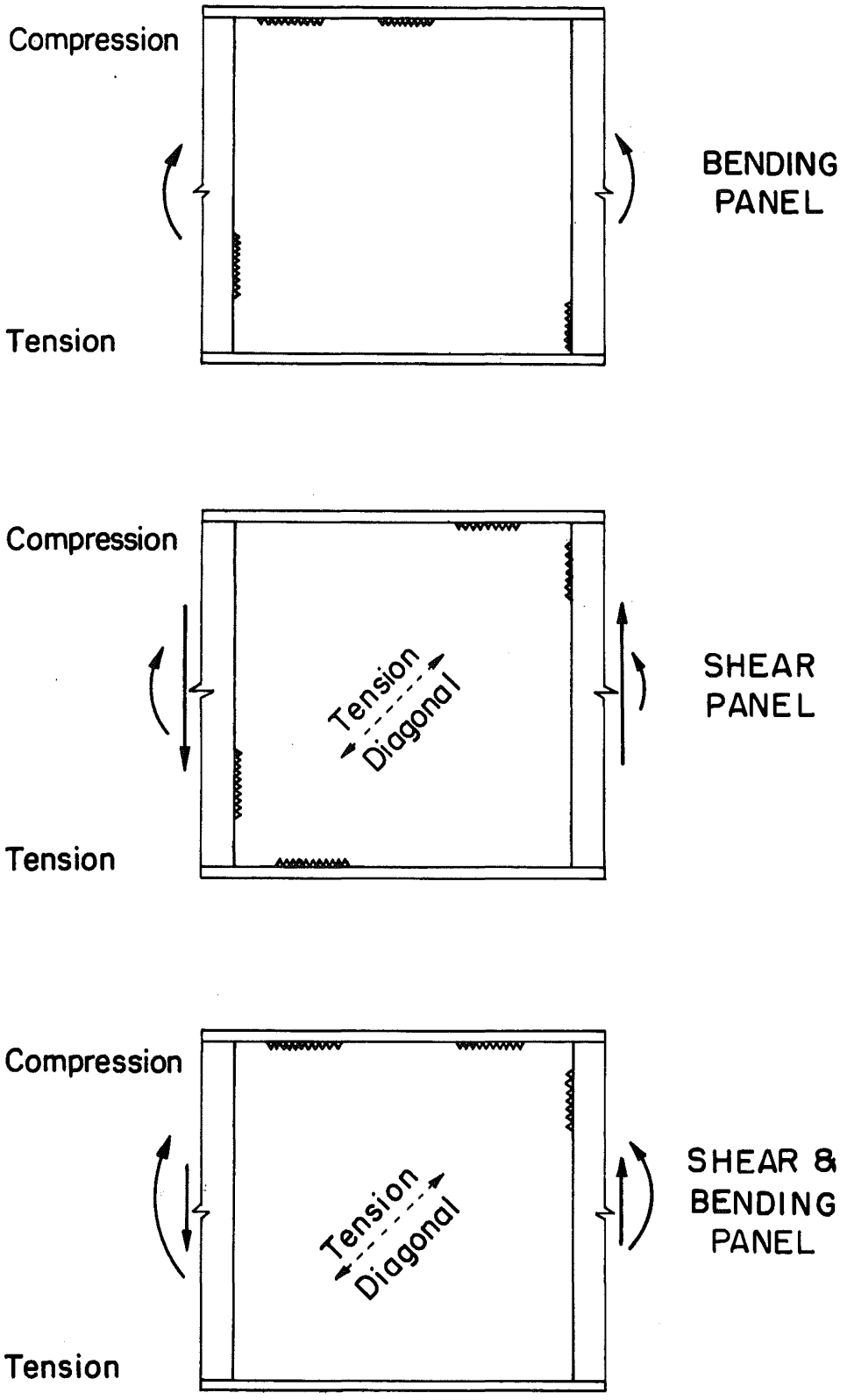

Fig. 5 Summary of Fatigue Crack Locations in Girder Webs

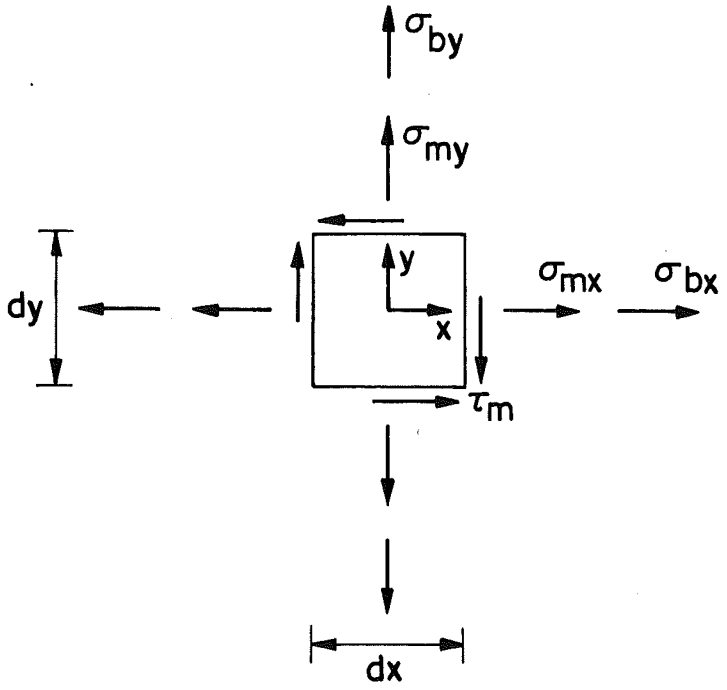

Fig. 6 State of Stress at Girder Web Boundary

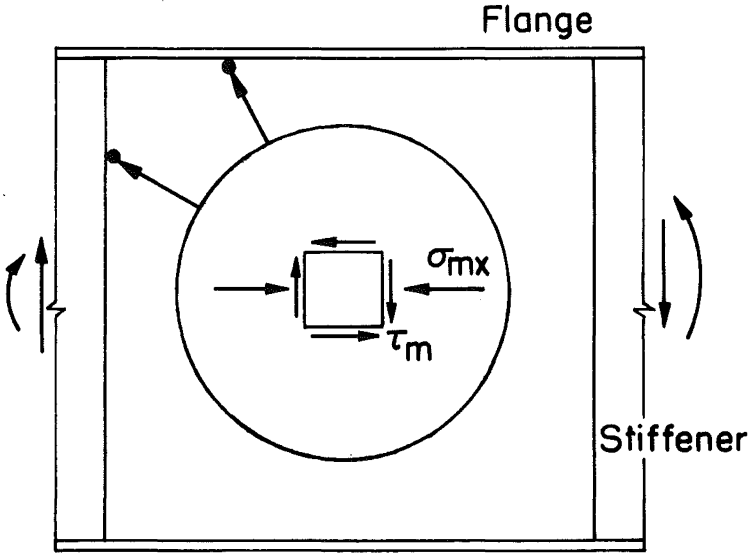

Fig. 7 Beam Theory Stresses in Girder Webs

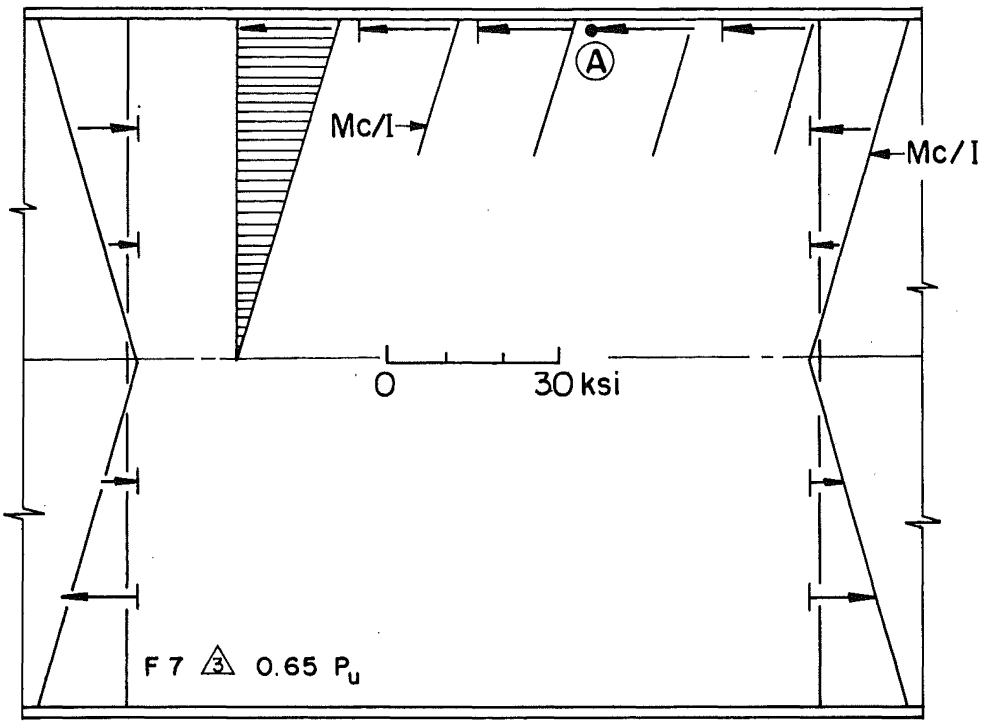

(a) Normal Stress (σ_{mx})

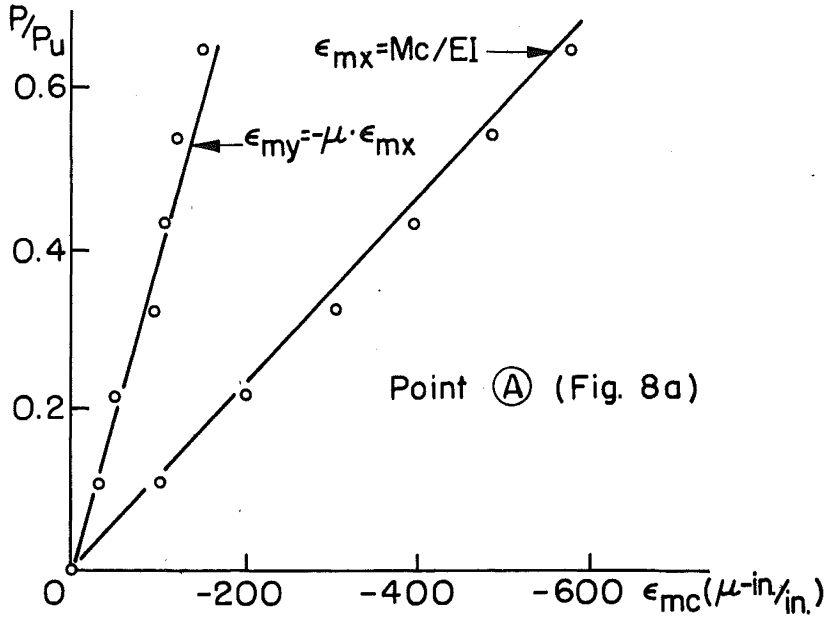

(b) Membrane Strains Normal and Parallel to Flange

Fig. 8 Web Membrane Stresses and Strains from Measurements - Bending Panel

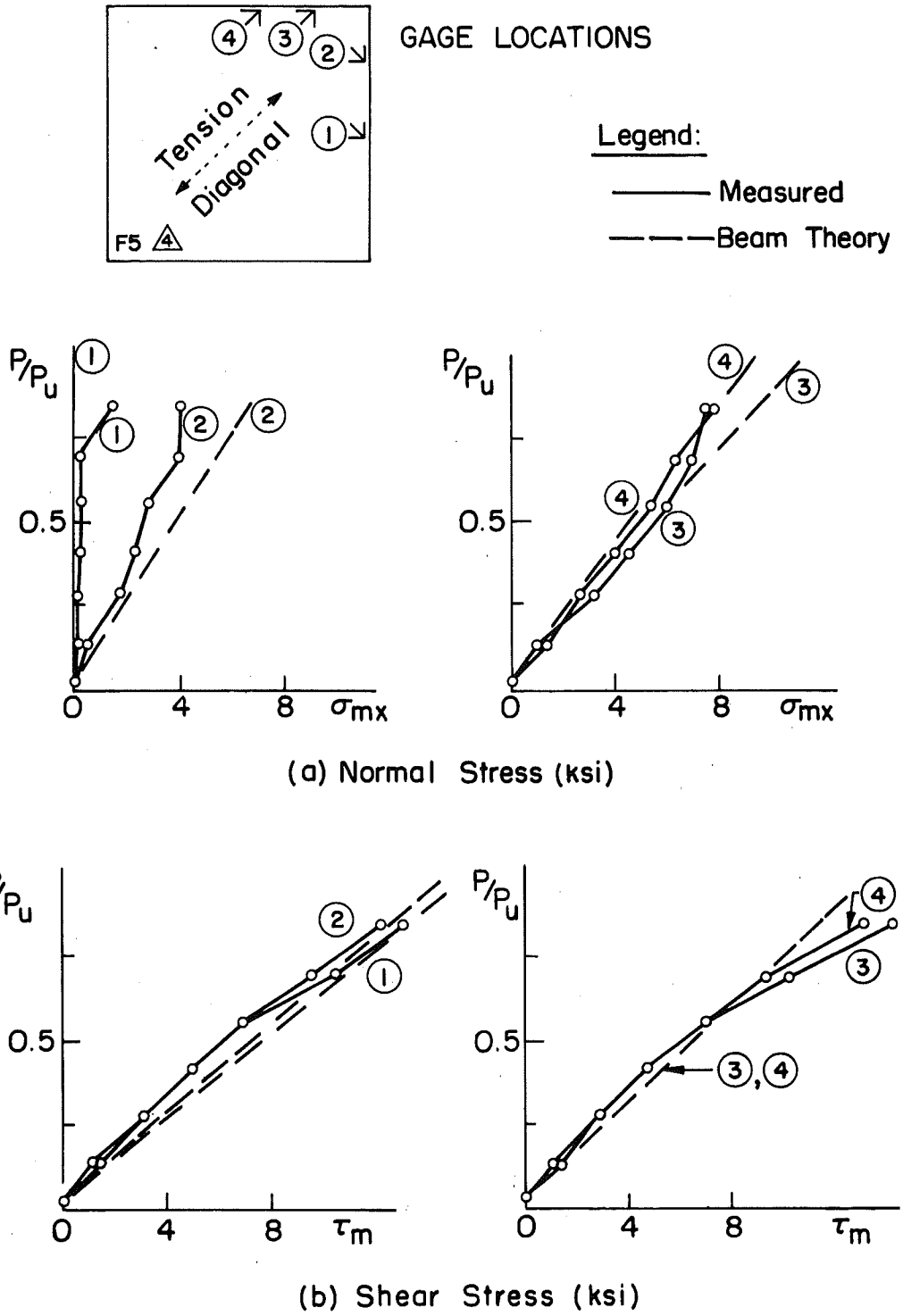

Fig. 9 Web Membrane Stresses from Measured Strains - Shear Panel

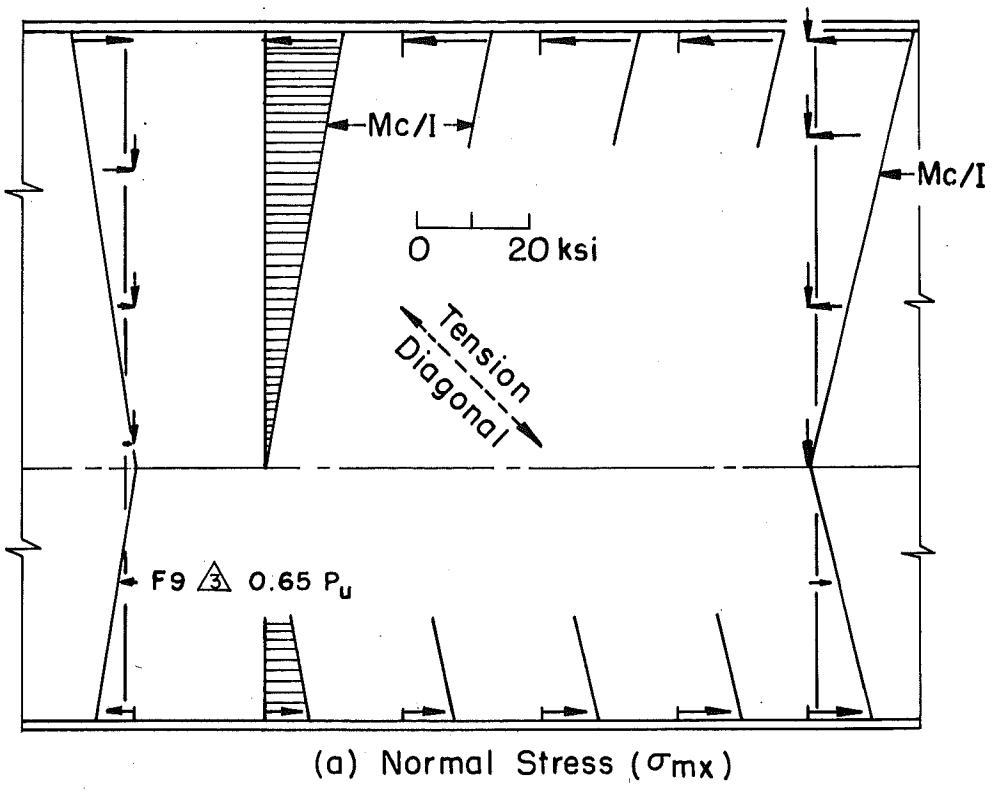

(a) Normal Stress (σ_{mx})

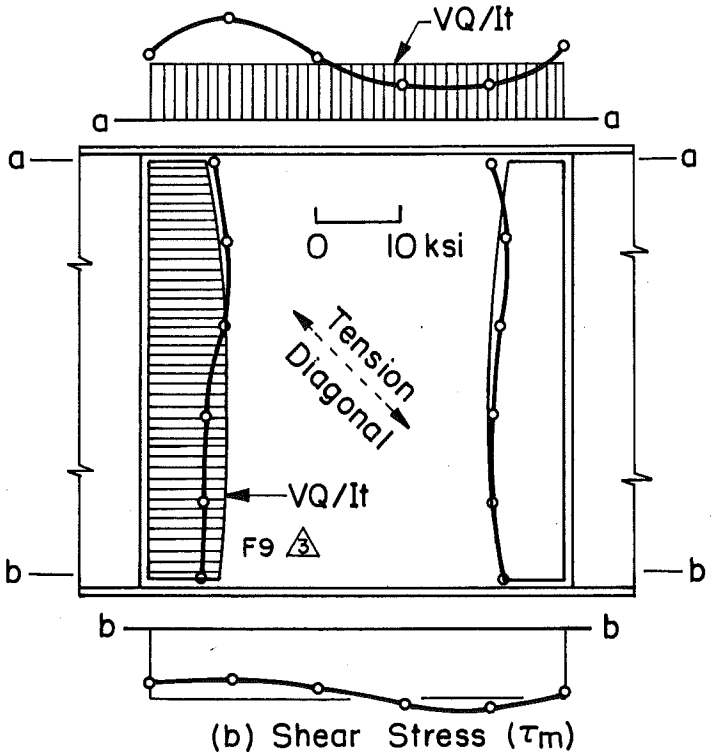

(b) Shear Stress (τ_m)

Fig. 10 Web Membrane Stresses from Measured Strains - Panel Under Bending and Shear

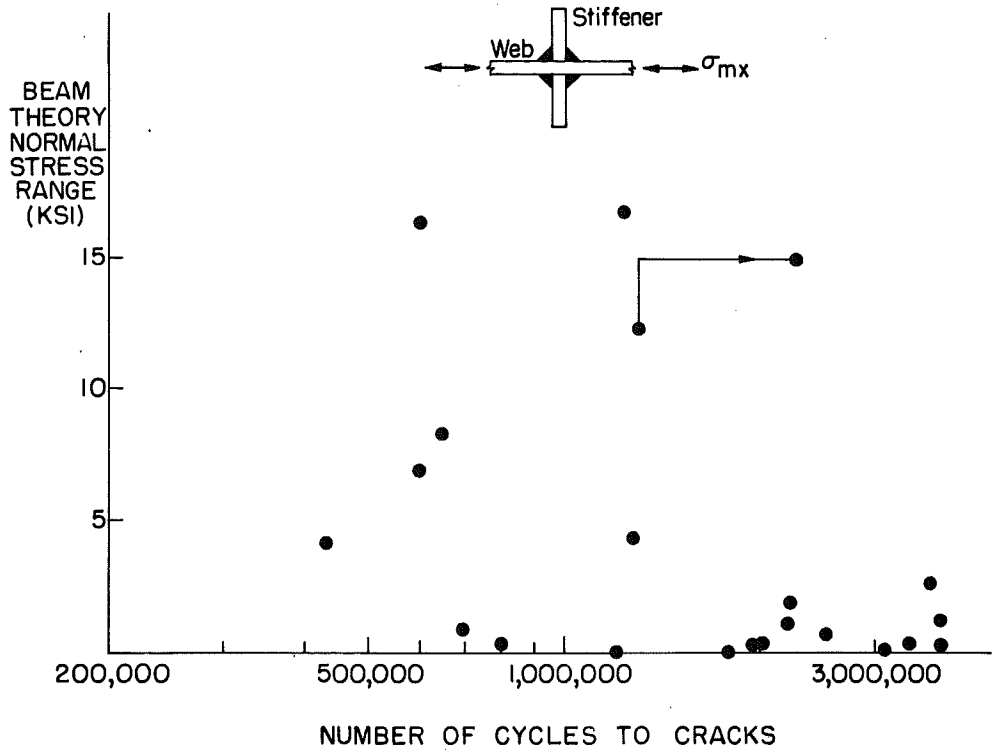

Fig. 11 Beam Theory Normal Stress Versus Number of Cycles to Cracks Along Stiffeners

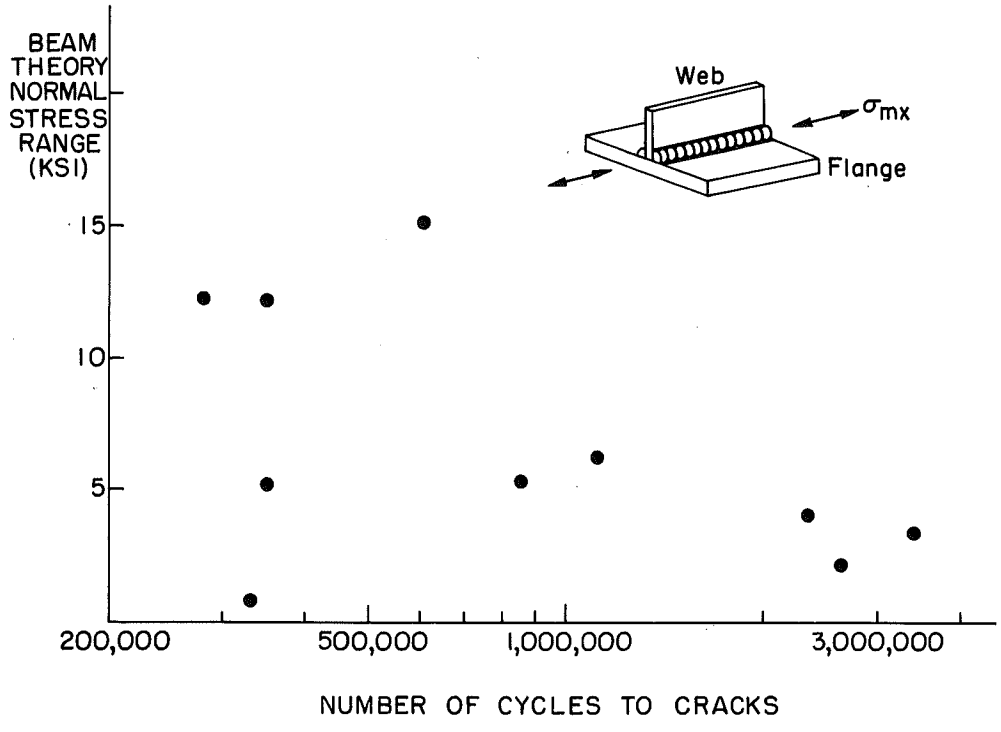

Fig. 12 Beam Theory Normal Stress Versus Number of Cycles to Cracks Along Flange

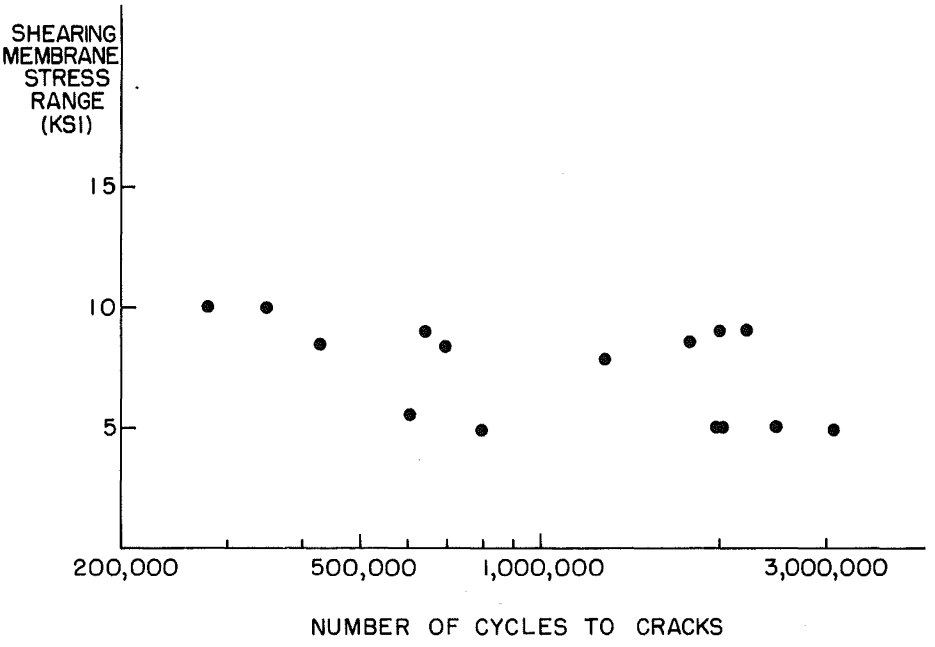

Fig. 13 Shearing Membrane Stress Versus Number of Cycles to Cracks

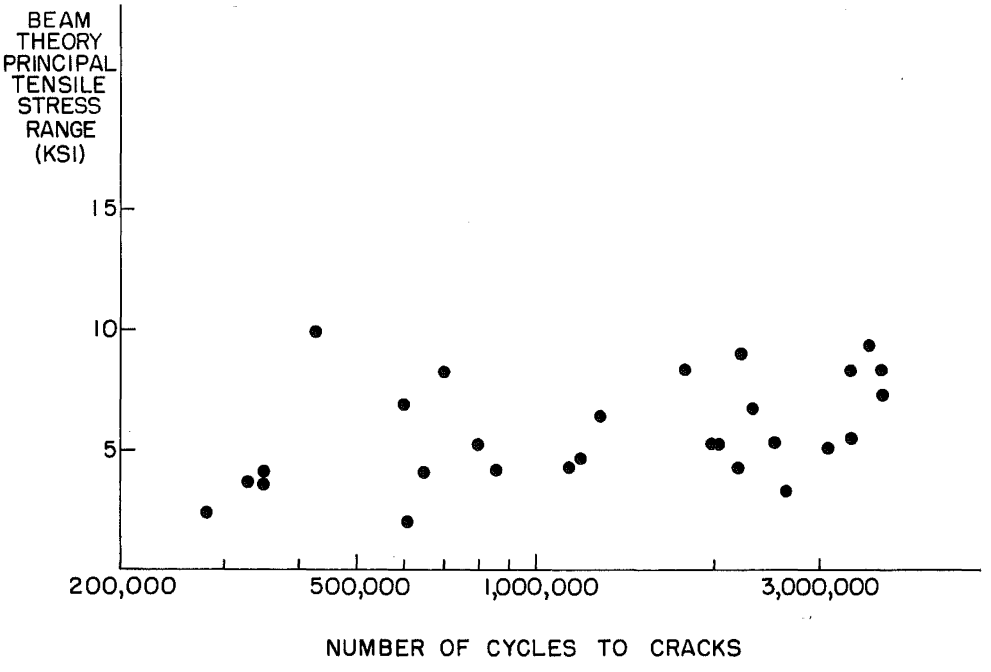

Fig. 14 Beam Theory Principal Tensile Stress Versus Number of Cycles to Cracks

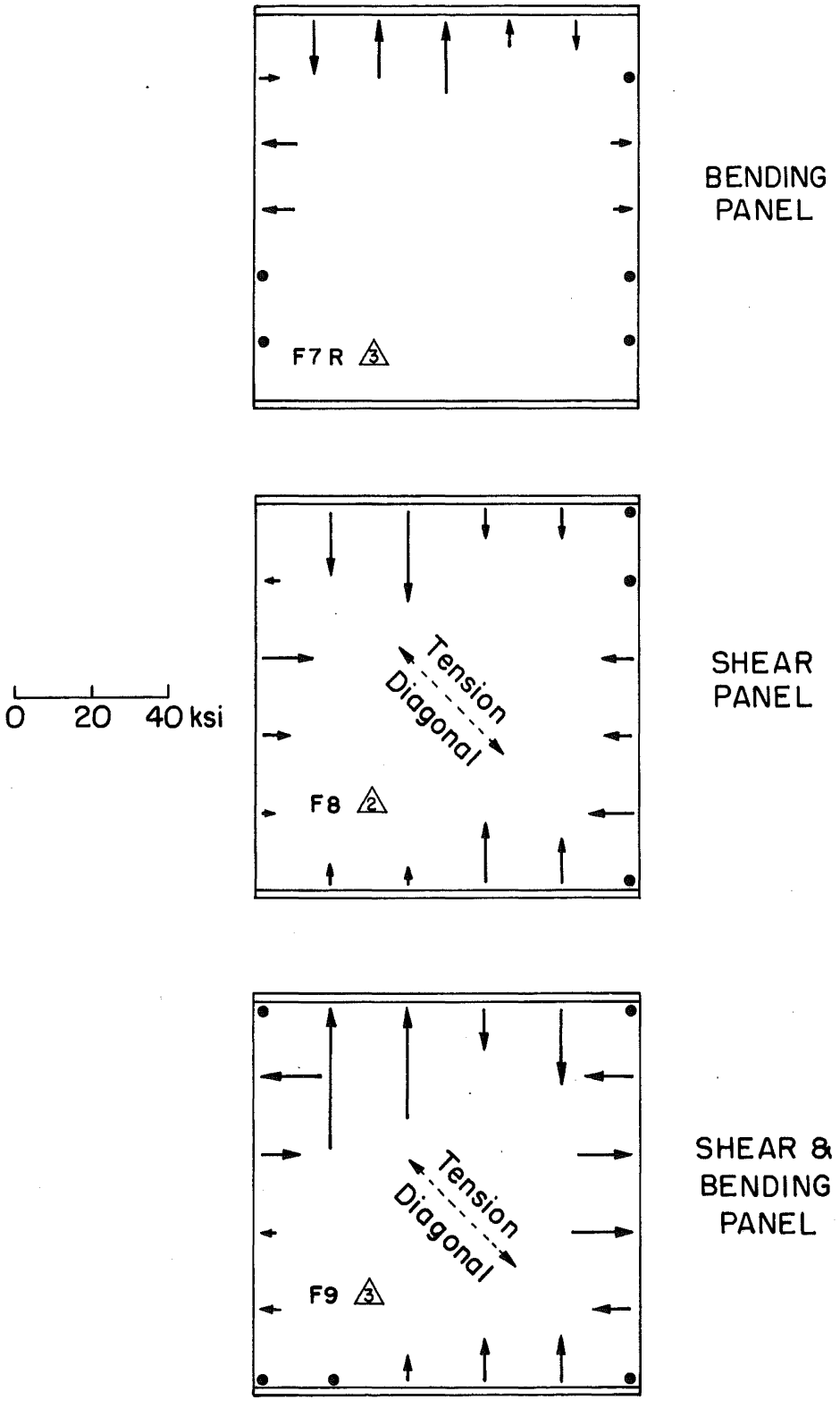

Fig. 15 Plate Bending Stresses from Measured Strains

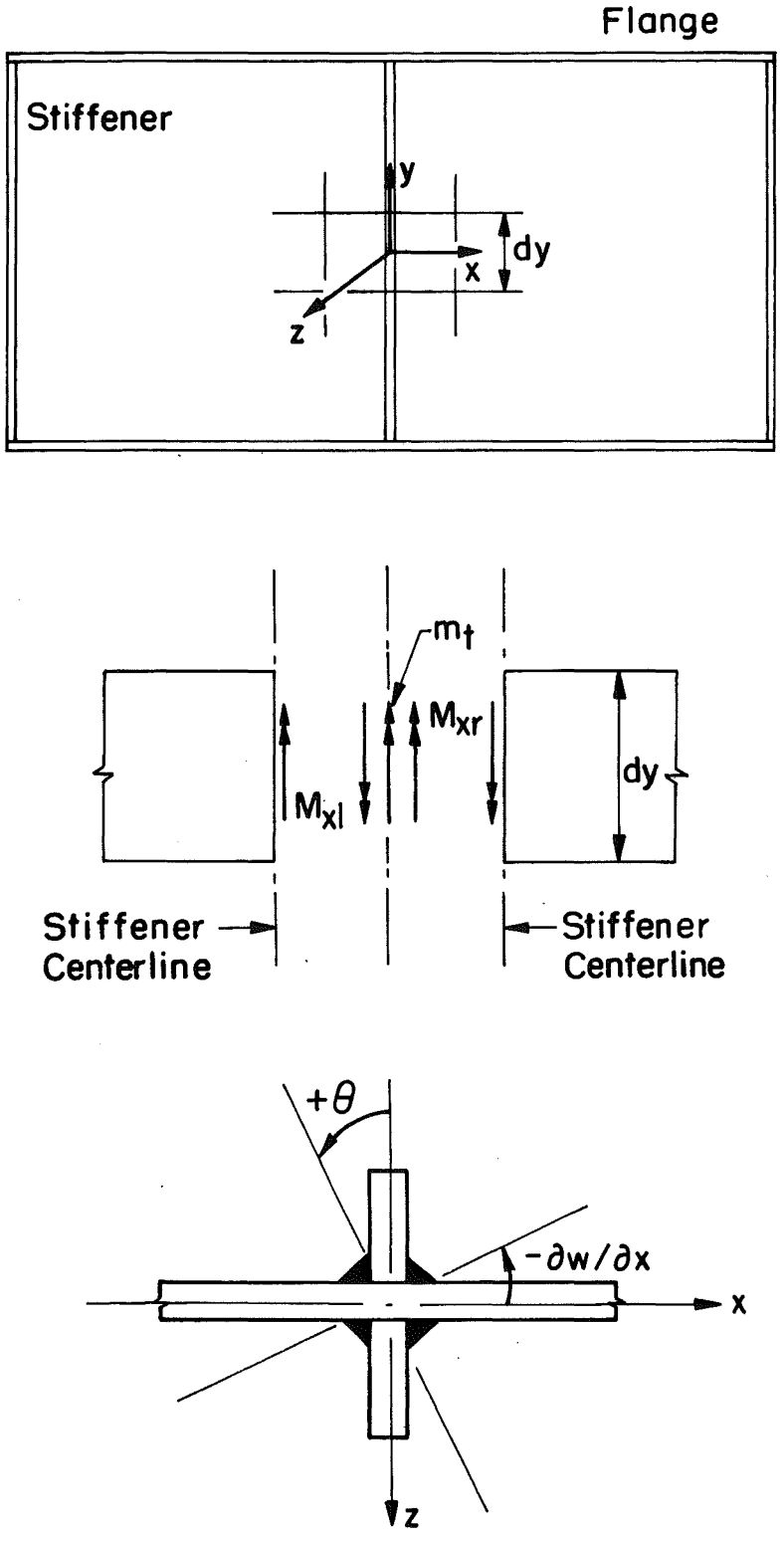

Fig. 16 Equilibrium and Compatibility Conditions for Stiffener-to-Web Joint

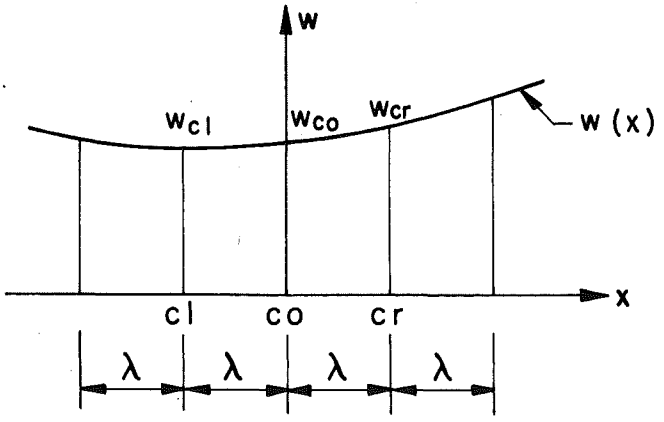

(a) Deflections

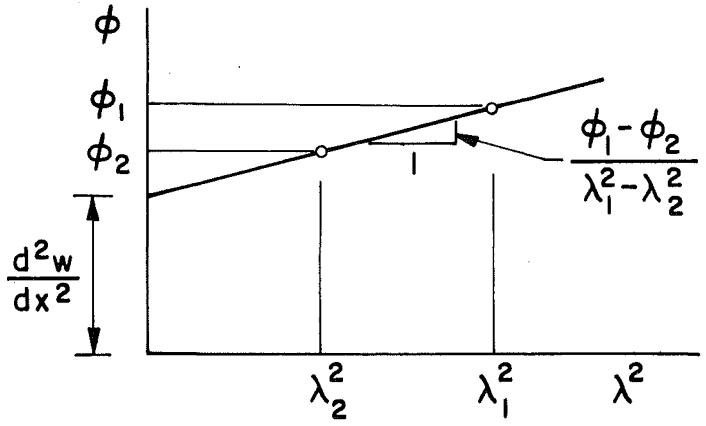

(b) Linear Extrapolation

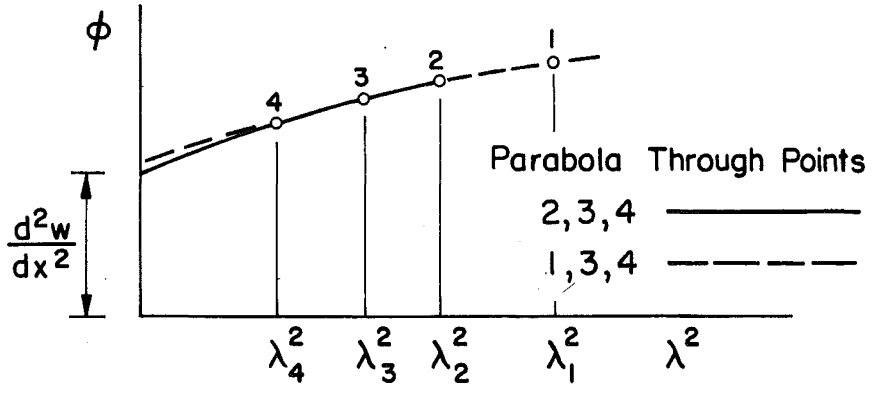

(c) Parabolic Extrapolation

Fig. 17 Finite Difference Extrapolation

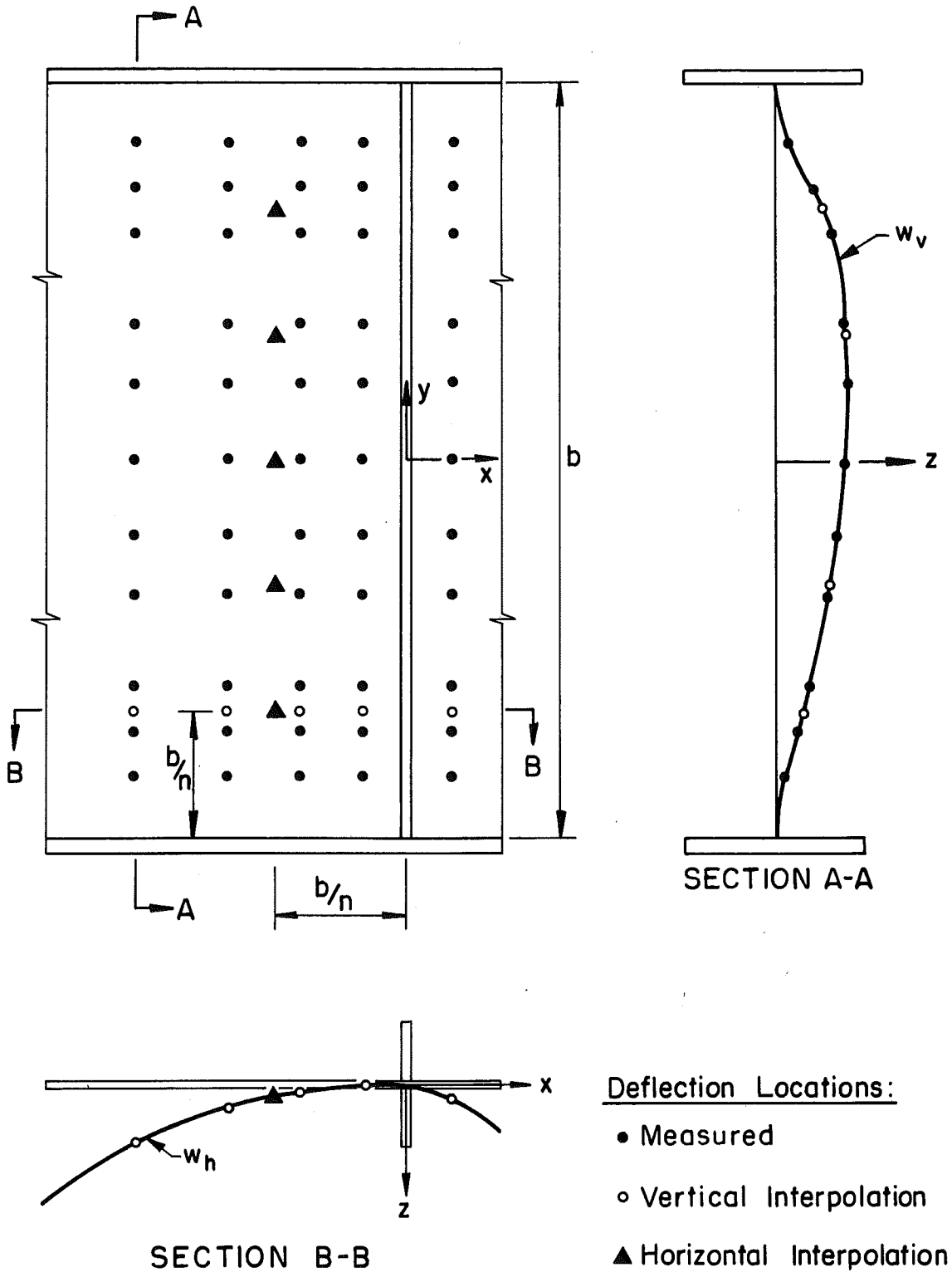

Fig. 18 Locations of Measured and Interpolated Web Deflections

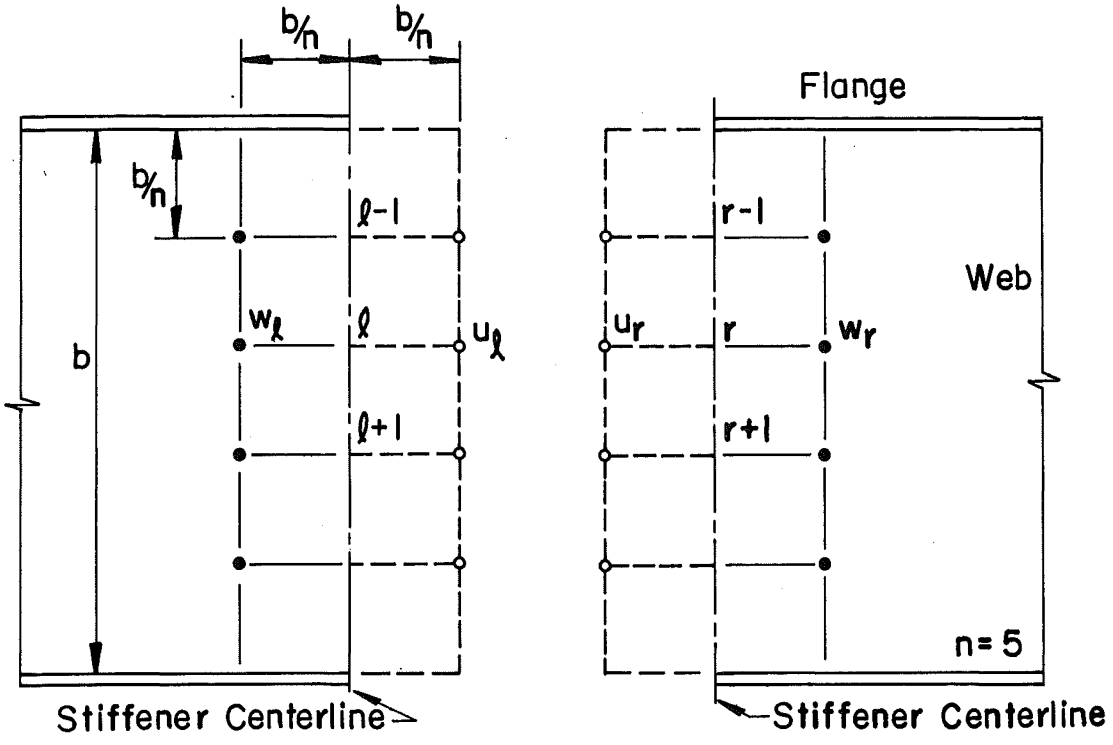

Fig. 19 Location of Real and Imaginary Deflections for Finite Differences

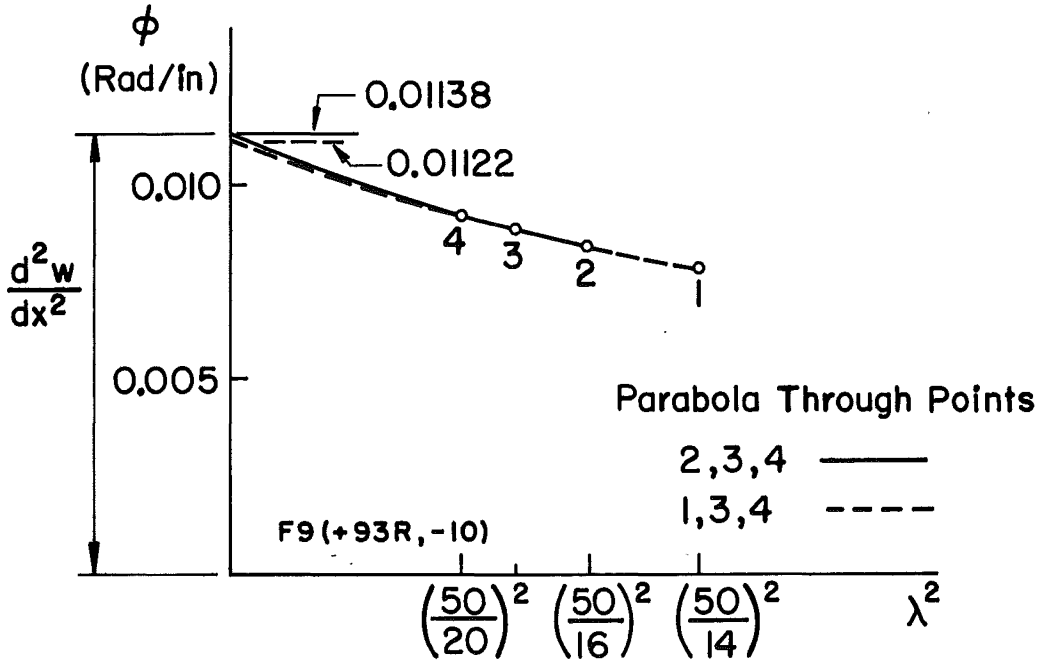

Fig. 20 Example of Finite Difference Extrapolation

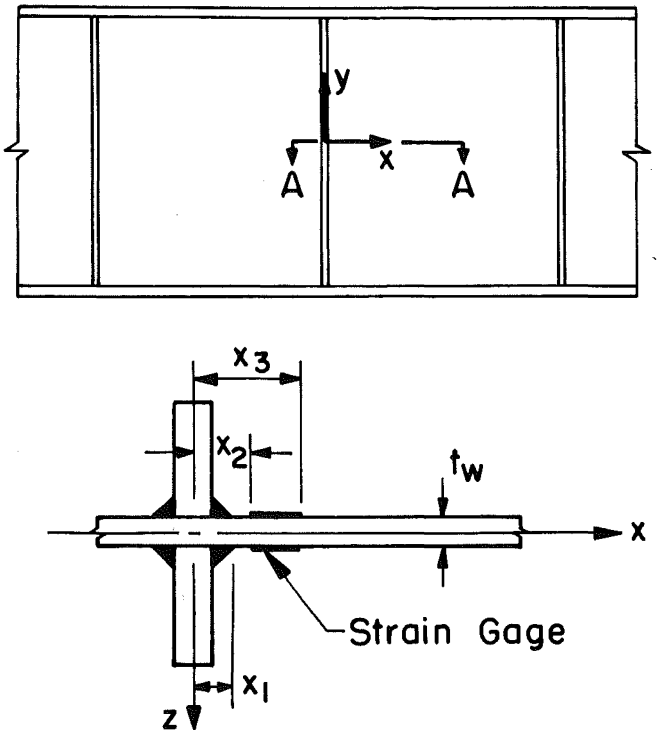

(a) Before Loading

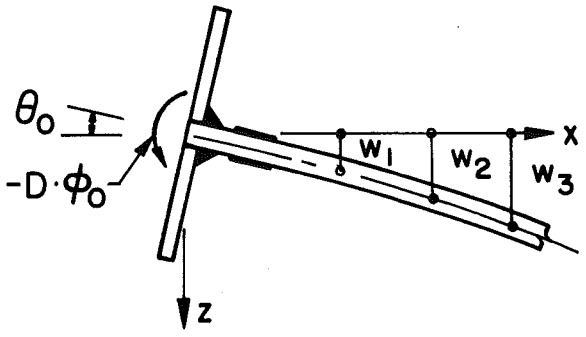

(b) After Loading

Fig. 21 Section through Stiffener-to-Web Joint

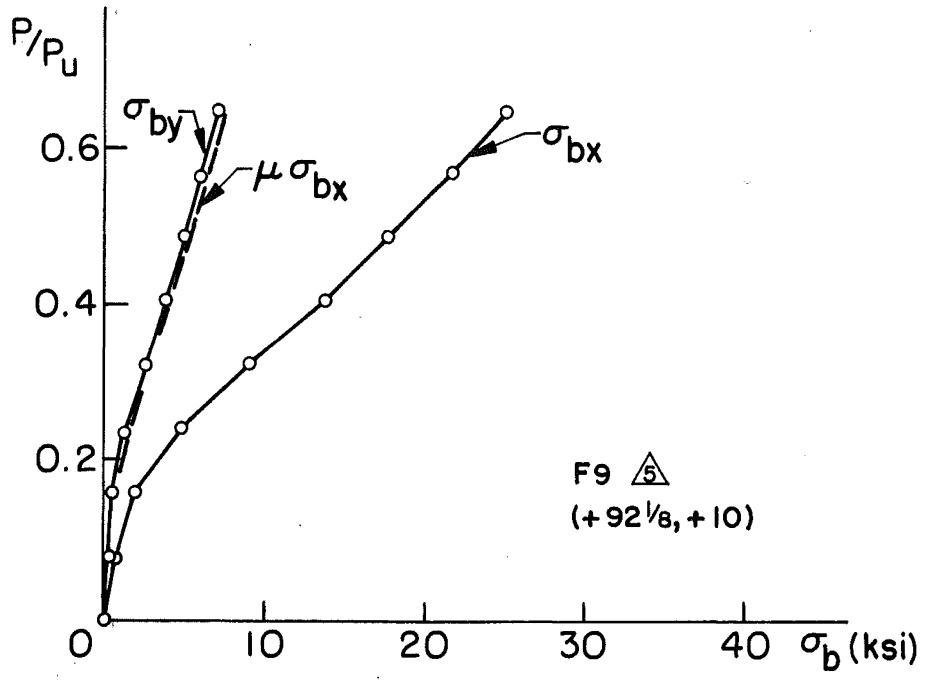

(a) Stresses at Stiffener

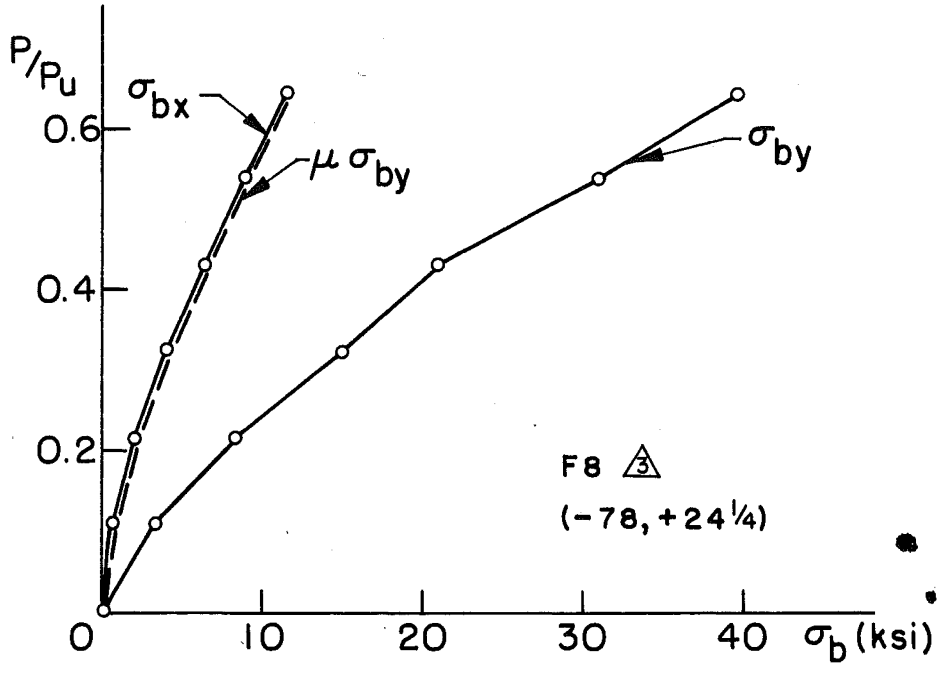

(b) Stresses at Flange

Fig. 22 Plate Bending Stresses Perpendicular and Parallel to Web Boundaries

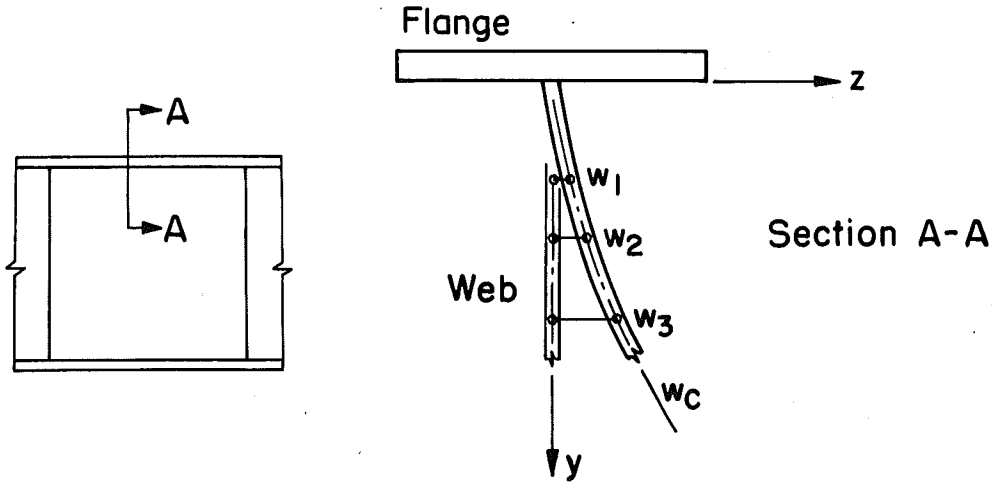

Fig. 23 Cantilever Strip Model for Flange Stress

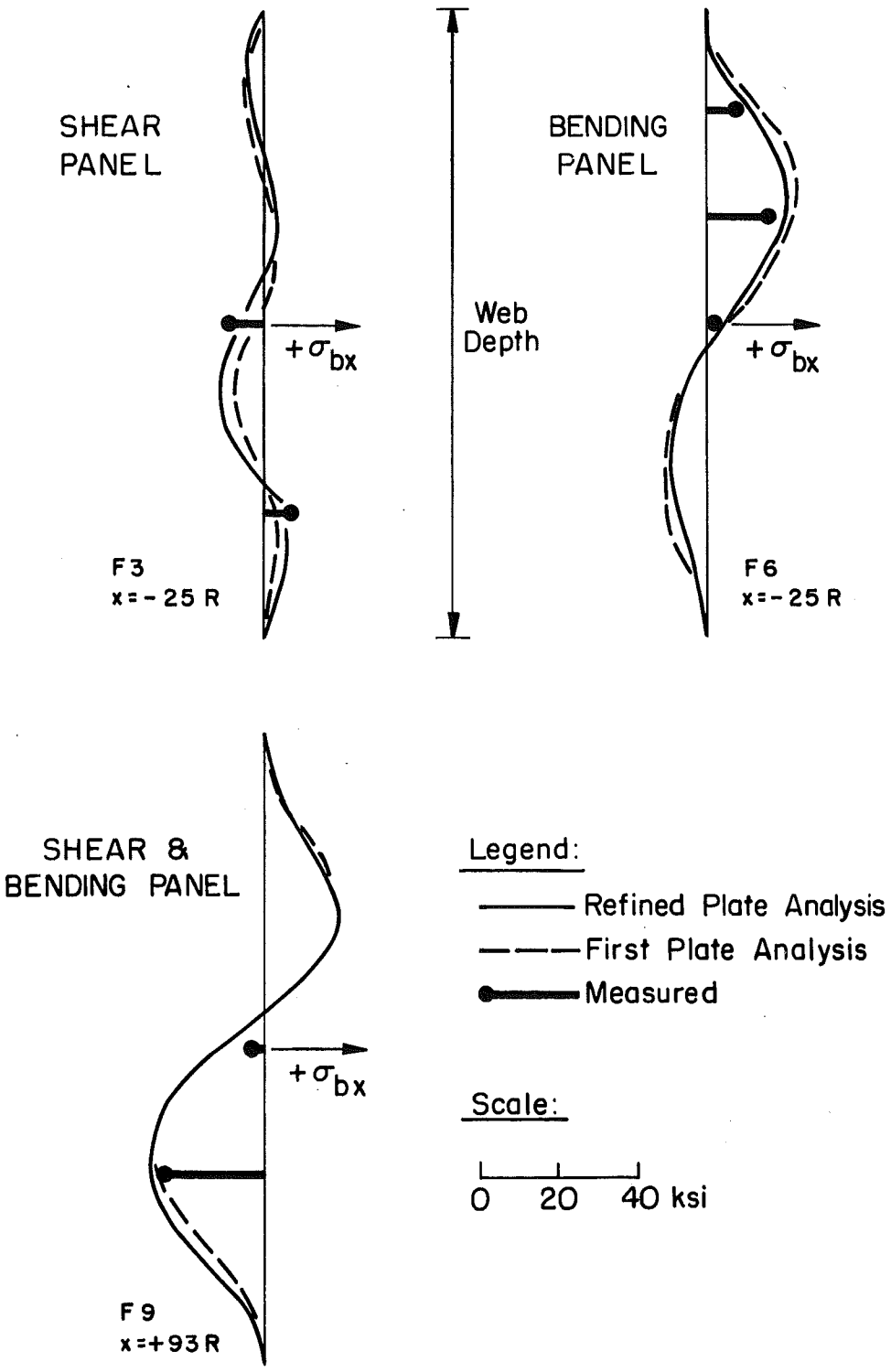

Fig. 24 Comparison Between Calculated and Measured Gage Stresses Along Stiffeners

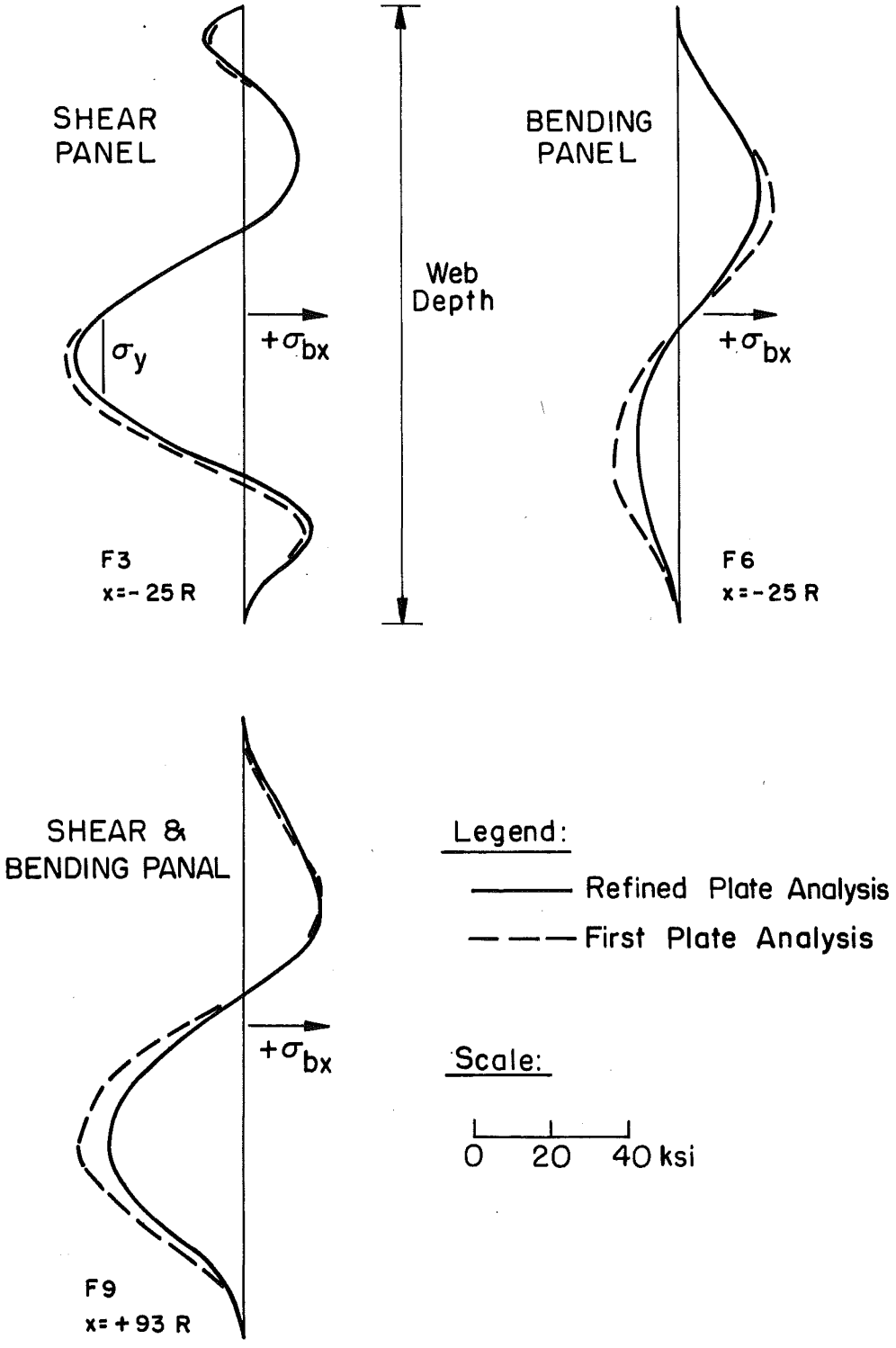

Fig. 25 Plate Bending Stresses at Toe of Fillet Weld Along Stiffener

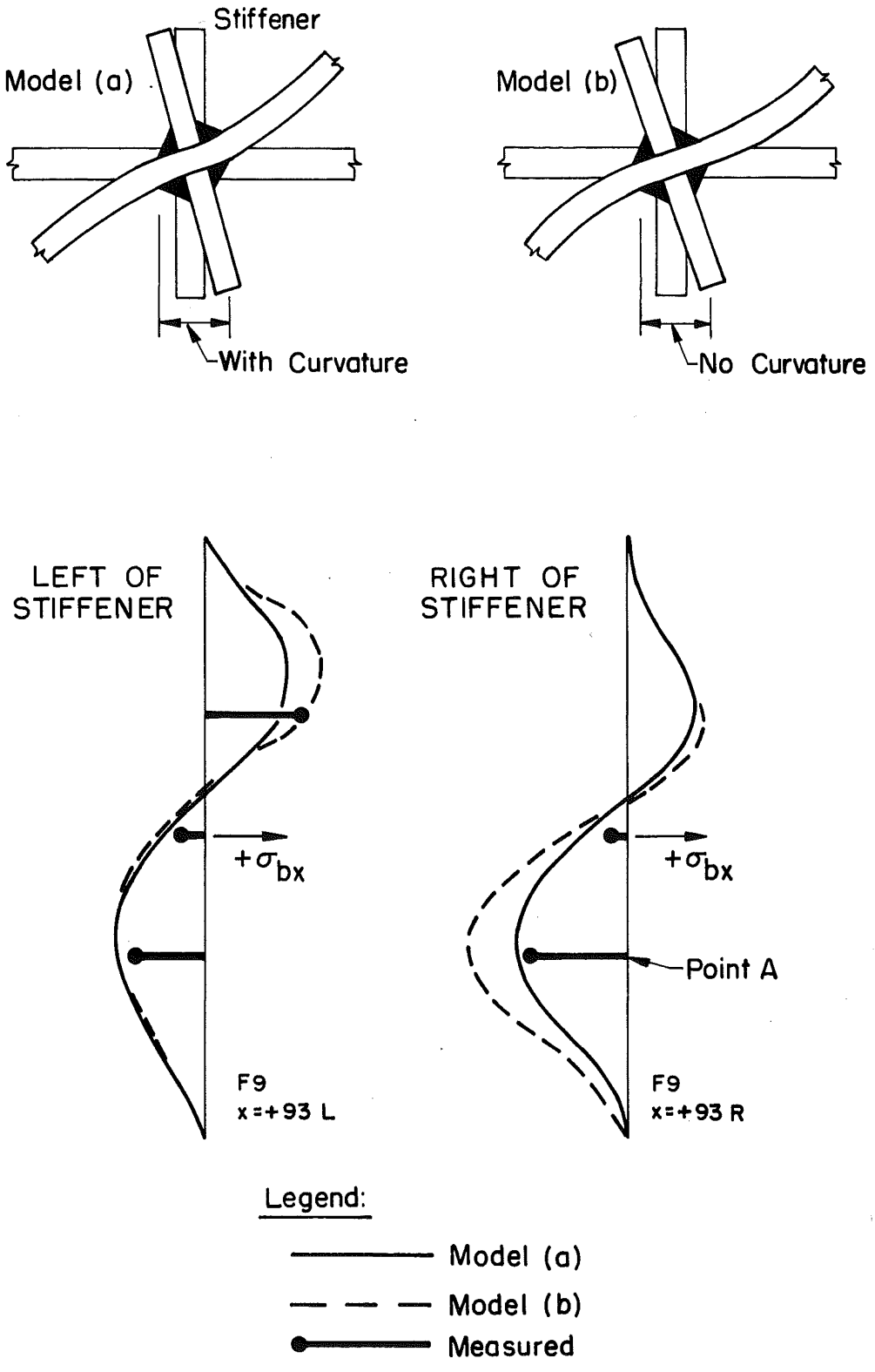

Fig. 26 Comparison Between Calculated and Measured Gage Stresses for Two Web-to-Stiffener Models

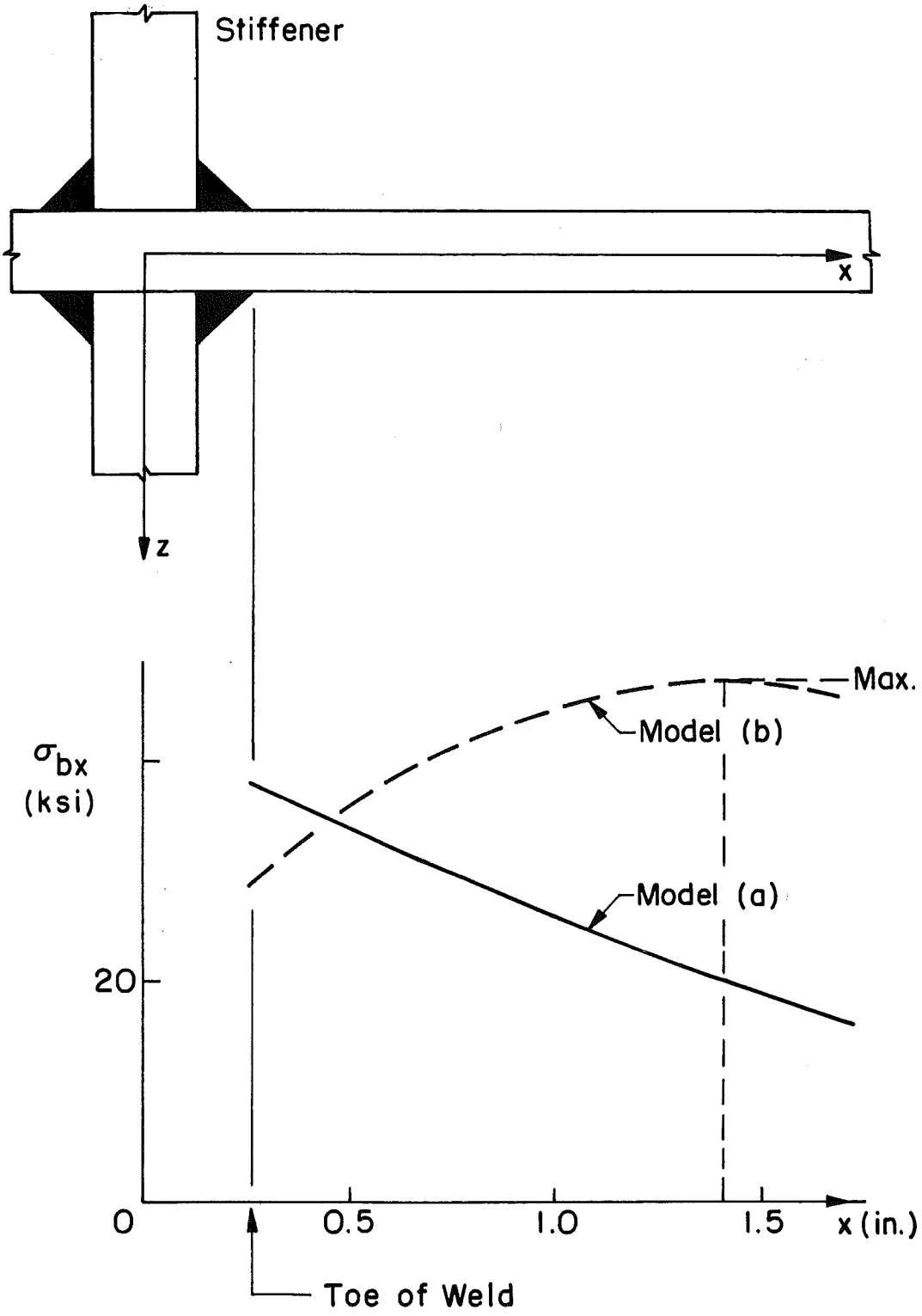

Fig. 27 Longitudinal Variation of Plate Bending Stress for Two Web-to-Stiffener Models

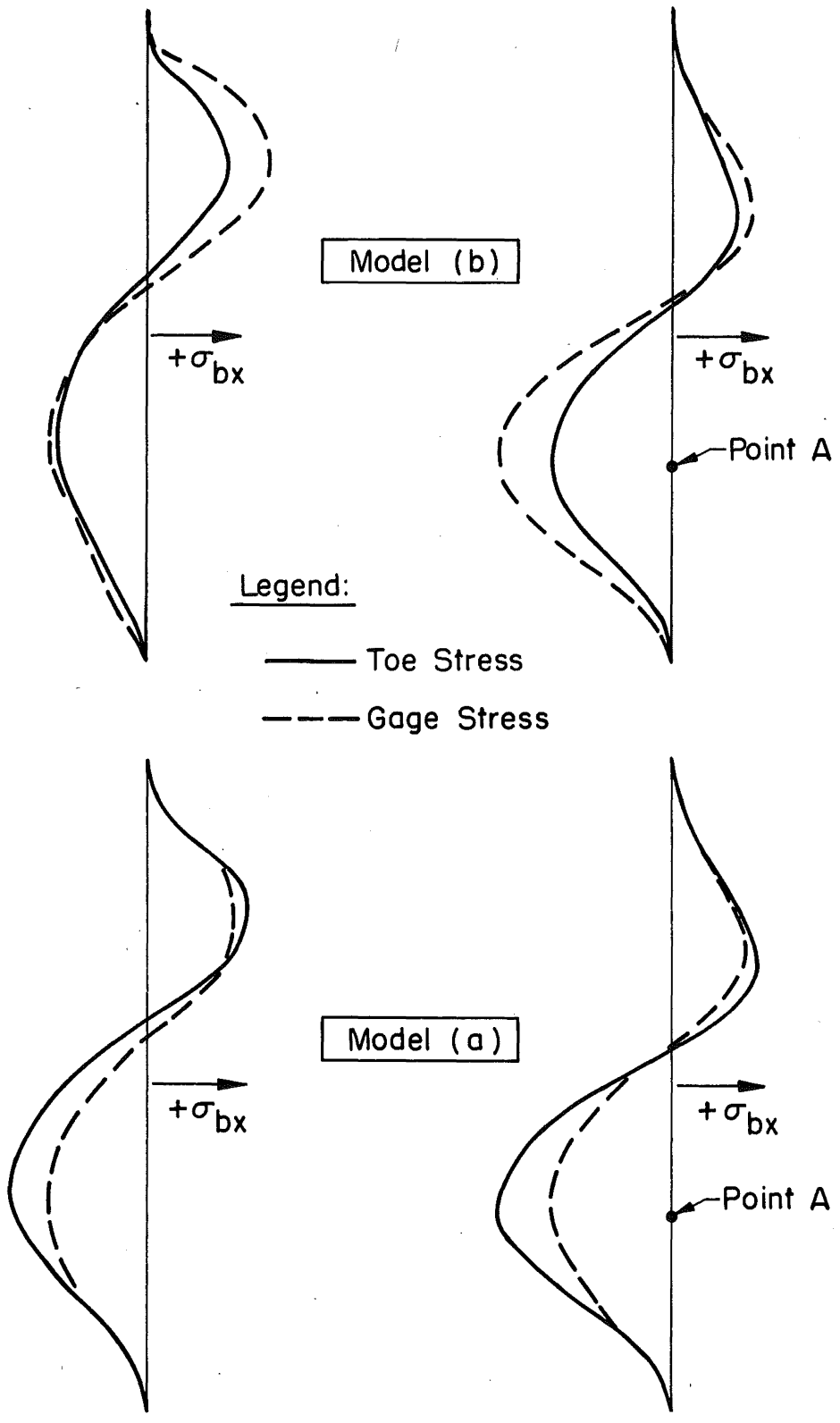

Fig. 28 Comparison Between Plate Bending Stresses at Gage and at Toe of Fillet Weld for Two Web-to-Stiffener Models

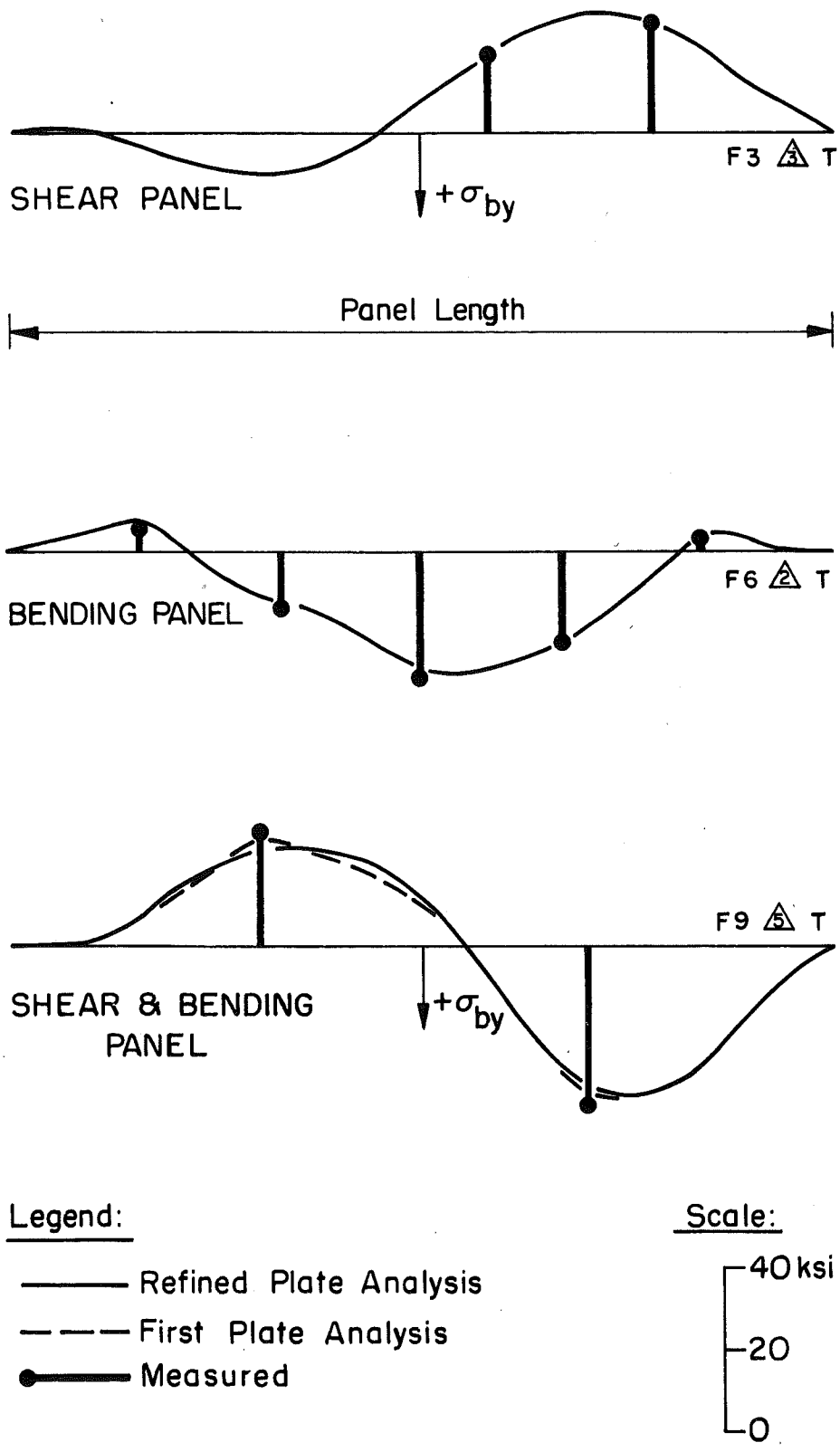

Fig. 29 Comparison Between Calculated and Measured Gage Stresses Along Flanges

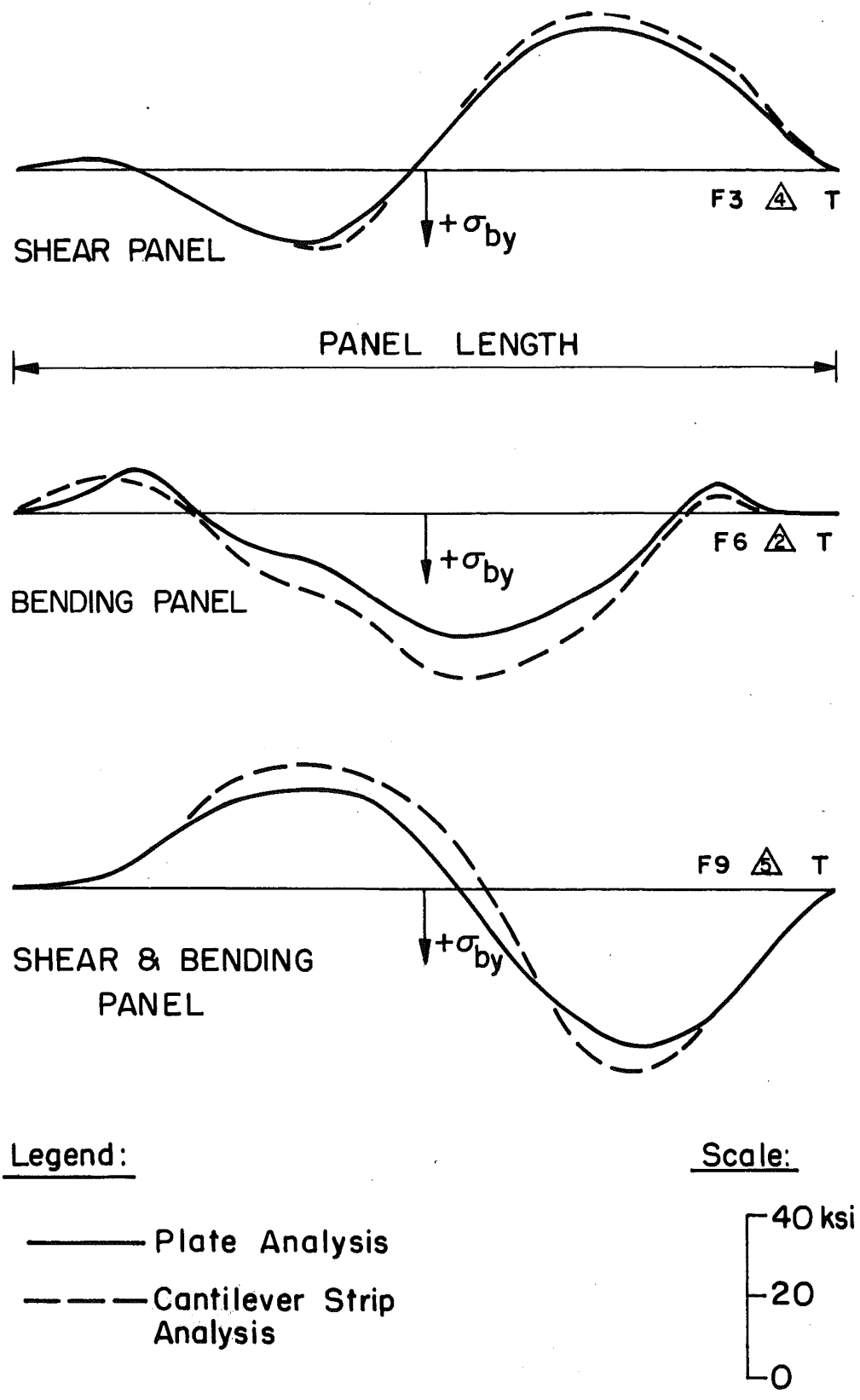

Fig. 30 Plate Bending Stresses at Toe of Fillet Weld Along Flanges

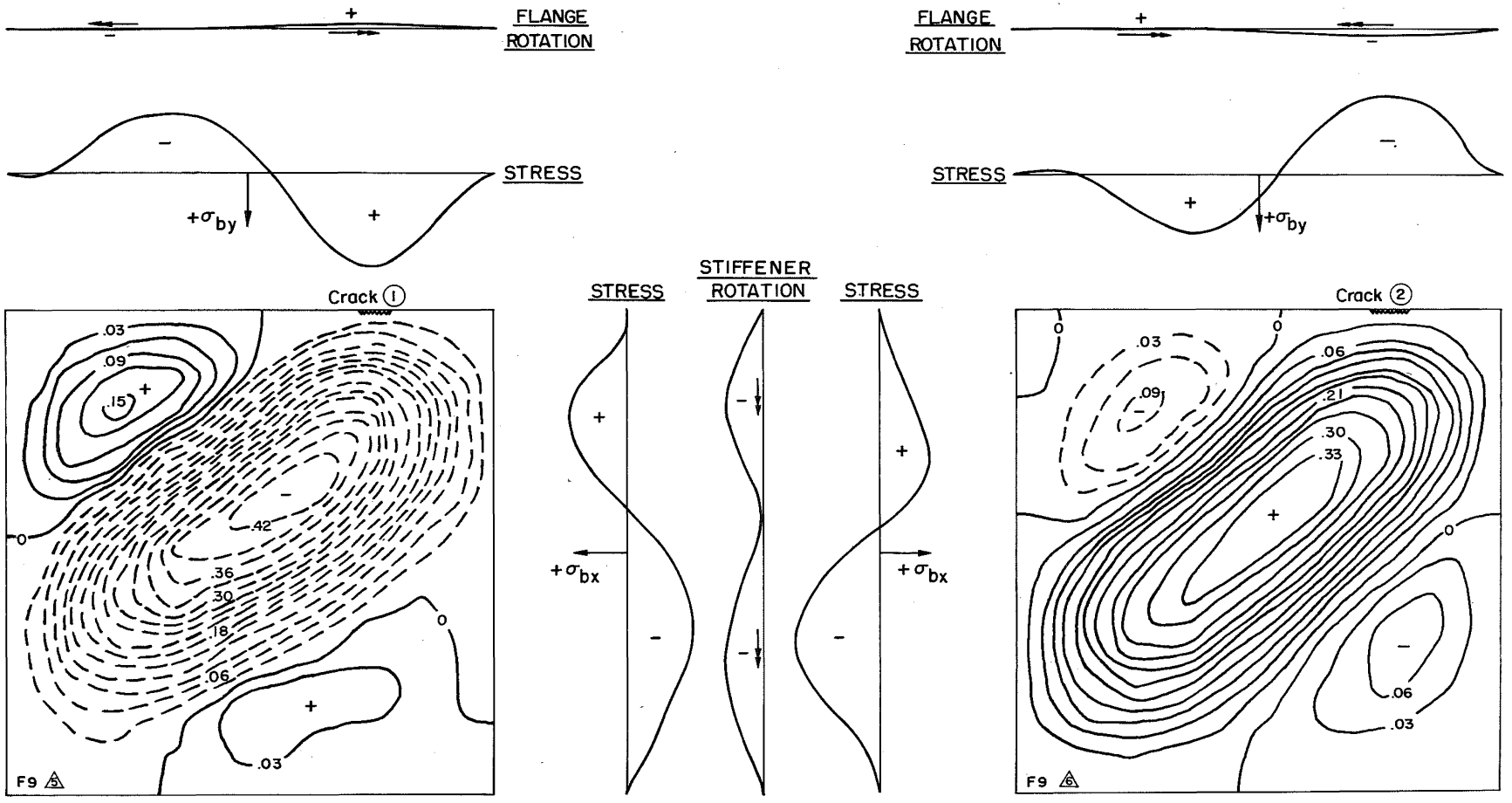

Fig. 31 Comparison of Lateral Web Deflections, Boundary Rotations and Plate Bending Stresses

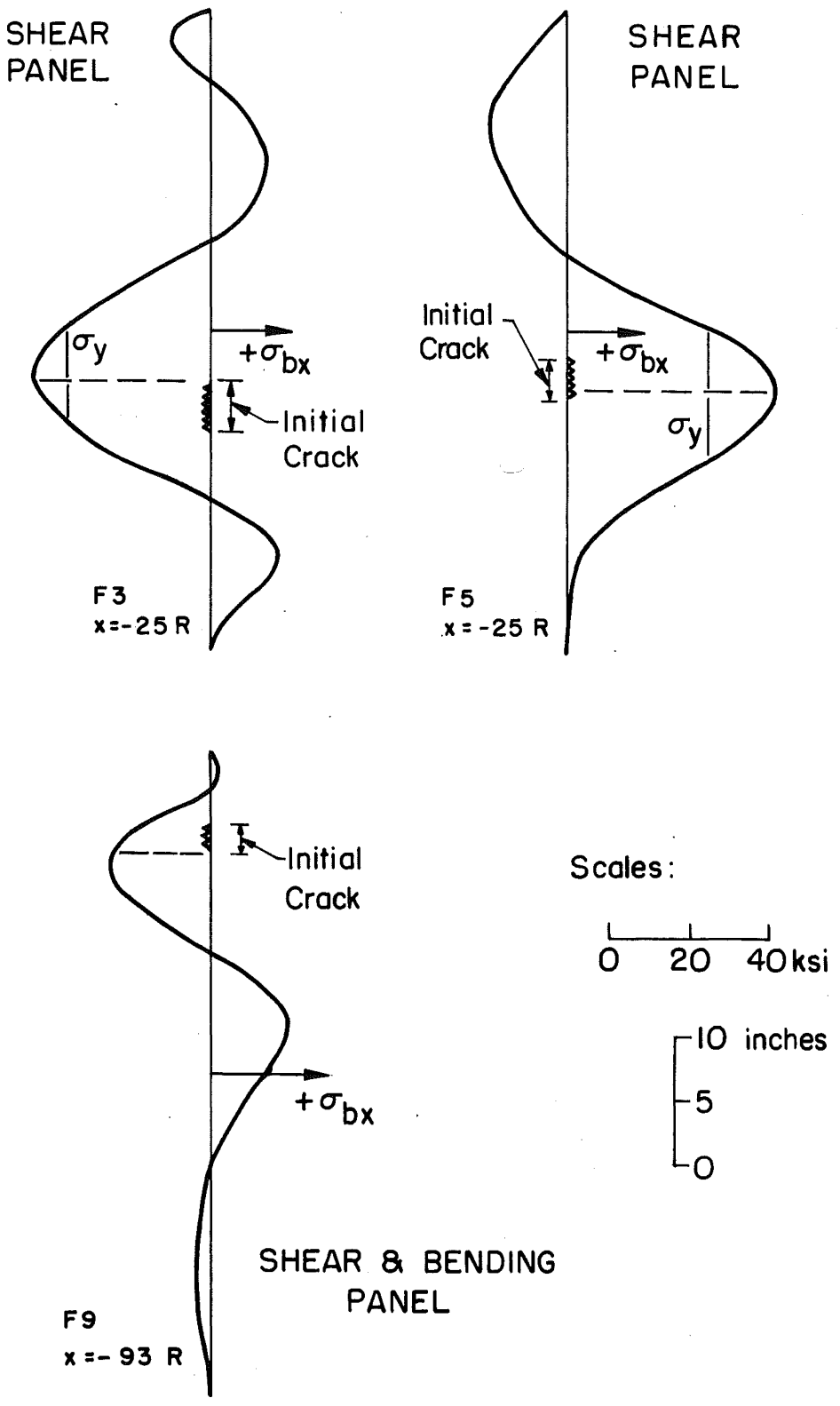

Fig. 32 Initial Cracks Compared with Plate Bending Stresses Along Stiffeners

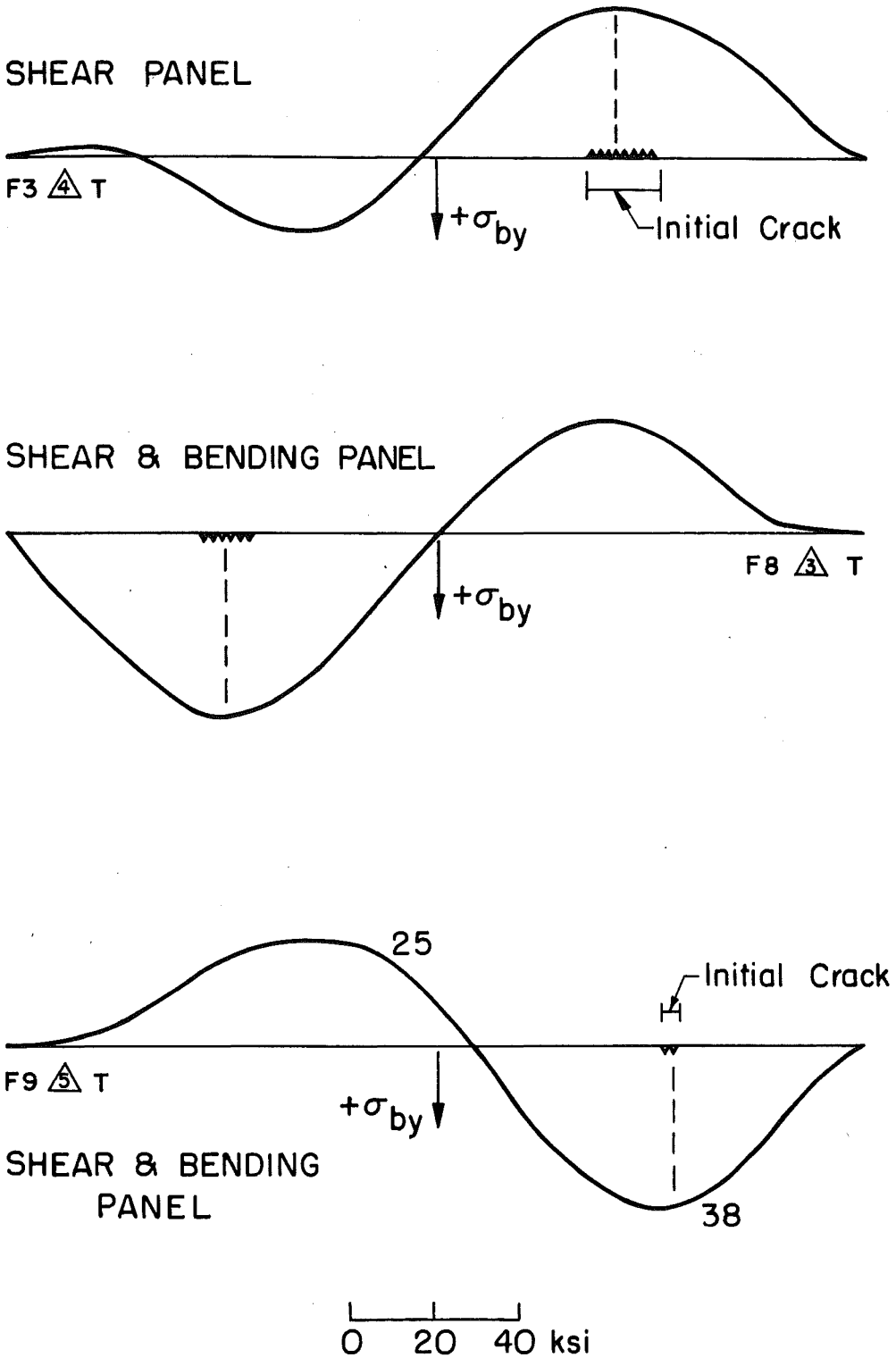

Fig. 33 Initial Cracks Compared with Plate Bending Stresses Along Flanges

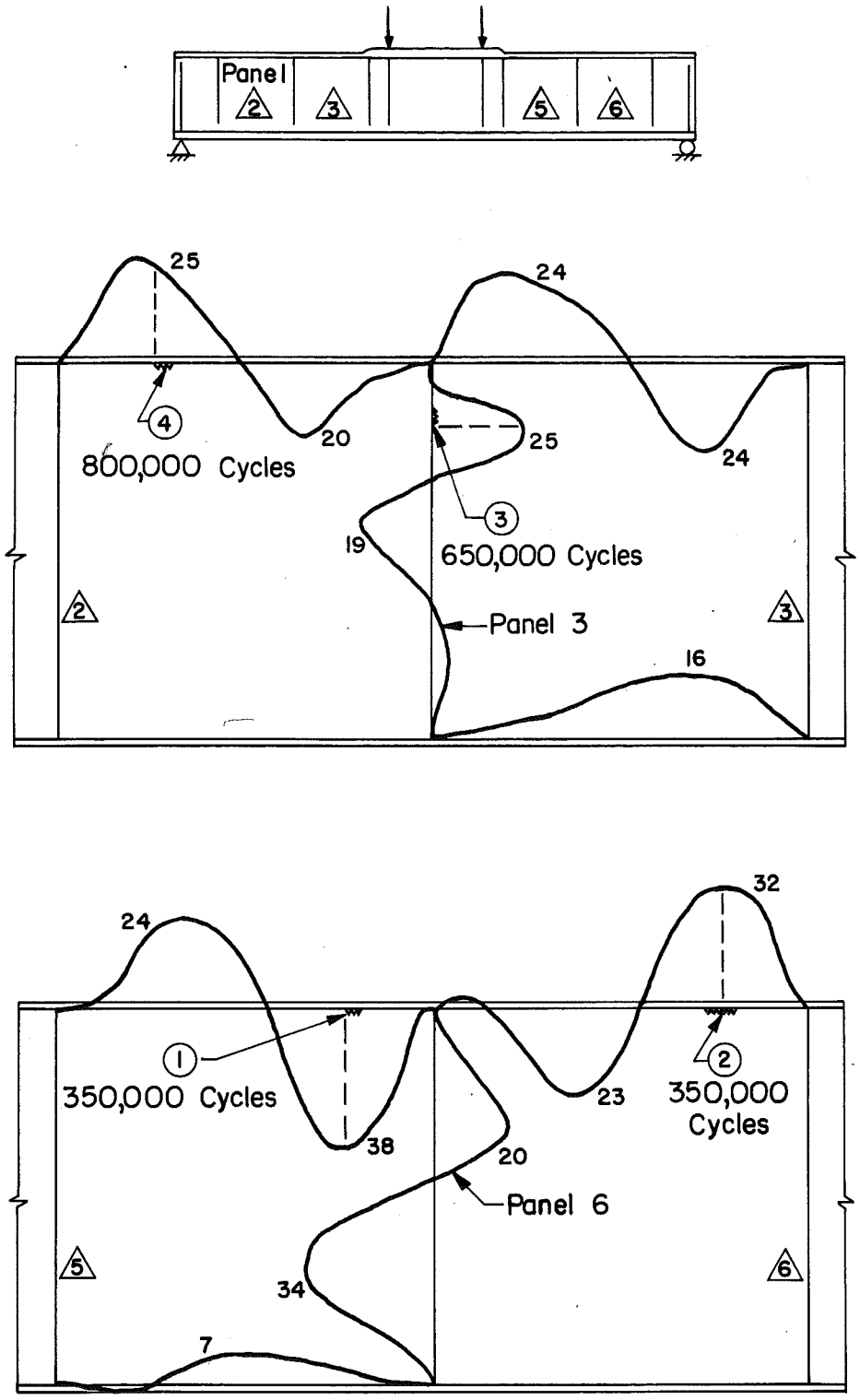

Fig. 34 Plate Bending Stresses Compared with Cracks on One Girder

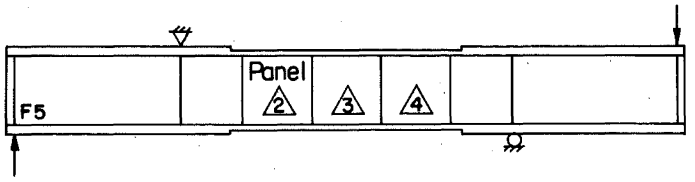

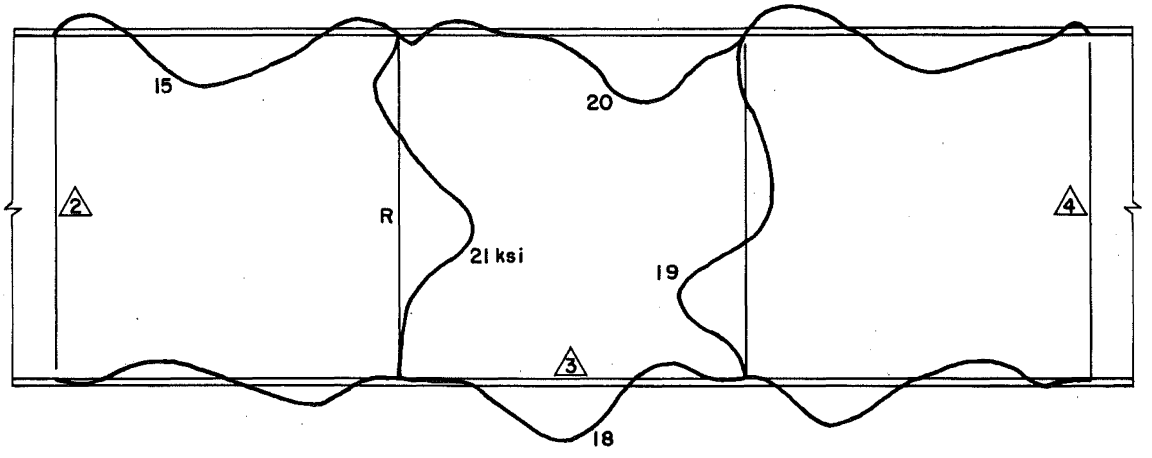

Fig. 35 Plate Bending Stresses for a Girder with no Cracks at 3,000,000 Cycles

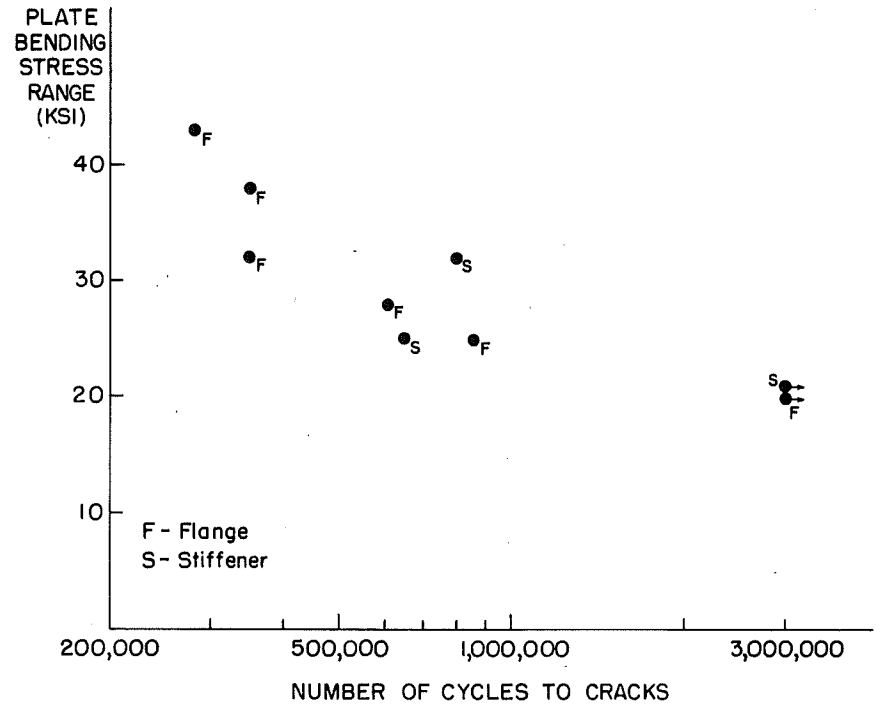

Fig. 36 Plate Bending Stress versus Number of Cycles to Cracks

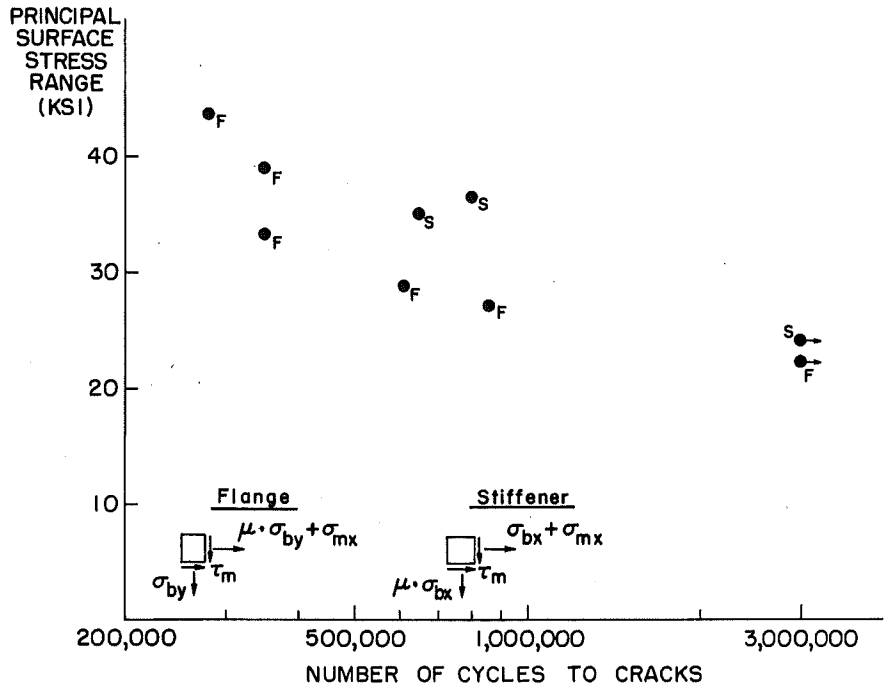

Fig. 37 Principal Surface Stress versus Number of Cycles to Cracks

REFERENCES

1. Basler, K., Yen, B. T., Mueller, J. A., and Thürlimann, B.
   WEB BUCKLING TESTS ON WELDED PLATE GIRDERS,
   Bulletin No. 64, Welding Research Council, New York,
   September 1960

2. Basler, K. and Thürlimann, B.
   STRENGTH OF PLATE GIRDERS IN BENDING,
   Proceedings, ASCE, Vol. 87, No. ST6, August 1961

3. Basler, K.
   STRENGTH OF PLATE GIRDERS IN SHEAR,
   Proceedings, ASCE, Vol. 87, No. ST7, October 1961

4. Basler, K.
   STRENGTH OF PLATE GIRDERS UNDER COMBINED BENDING AND SHEAR,
   Proceedings, ASCE, Vol. 87, No. ST7, October 1961

5. Yen, B. T. and Mueller, J. A.
   FATIGUE TESTS OF LARGE-SIZE WELDED PLATE GIRDERS,
   Bulletin No. 118, Welding Research Council, New York,
   November 1966

6. Goodpasture, D. W. and Stallmeyer, J. E.
   FATIGUE OF THIN-WEB STEEL GIRDERS,
   University of Illinois, April 1966 (Status Report to the
   Fatigue Committee of the Welding Research Council)

7. Lew, H. S. and Toprac, A. A.
   FATIGUE STRENGTH OF HYBRID PLATE GIRDERS UNDER CONSTANT
   MOMENT,
   Highway Research Record, No. 167, 1967

8. Dudley, K. E., Mueller, J. A. and Yen, B. T.
   LATERAL WEB DEFLECTIONS OF WELDED PLATE GIRDERS,
   Lehigh University, Fritz Engineering Laboratory Report
   No. 303.4, June 1966

9. Yen, B. T.
   ON THE FATIGUE STRENGTH OF WELDED PLATE GIRDERS,
   Lehigh University, Fritz Engineering Laboratory Report
   No. 303.1, 1963

10. Hall, L. R. and Stallmeyer, J. E.
    THIN WEB GIRDER FATIGUE BEHAVIOR AS INFLUENCED BY BOUNDARY
    RIGIDITY,
    University of Illinois, Structural Research Series No. 278,
    January 1964

REFERENCES (continued)

11. Munse, W. H. and Grover, L.
FATIGUE OF WELDED STEEL STRUCTURES,
Welding Research Council, New York, 1964

12. Grover, H. J., Gordon, S. A., and Jackson, L. R.
THE FATIGUE OF METALS AND STRUCTURES,
Department of the Navy, NAVWEPS 00-25-534, 1954
(revised June 1960)

13. Gurney, T. R.
FATIGUE STRENGTH OF FILLET WELDED JOINTS IN STEEL,
British Welding Journal, Vol. 7, No. 3, March 1960

14. Fisher, J. W. and Viest, I. M.
FATIGUE LIFE OF BRIDGE BEAMS SUBJECTED TO CONTROLLED TRUCK TRAFFIC,
Preliminary Publications, IABSE, August 1964

15. deLeiris, H. and Dutilleul, H.
FATIGUE TESTS OF ARC-WELDED JOINTS,
The Welding Journal, February 1952, p. 104-s

16. von Kármán, T.
FESTIGKEITSPROBLEME IM MASCHINENBAU,
Encyklopädie der Mathematischen Wissenshaften,
Vol. 4, Part 4, 1910

17. Marguerre, K.
ZUR THEORIE DER GEKRÜMMTEN PLATTE MIT GROSSER FORMÄNDERUNG,
Proceedings, Fifth International Congress for Applied Mechanics, Vol. 5, 1958

18. Sliter, G. E., Nikolai, R. T., and Boresi, A. P.
ELASTIC PLATES: ANNOTATED BIBLIOGRAPHY 1930-1962
University of Illinois, Engineering Experiment Station Technical Report No. 10, 1964

19. Timoshenko, S. P. and Gere, J. M.
THEORY OF ELASTIC STABILITY,
McGraw-Hill, 1961

20. Timoshenko, S. P.
STRENGTH OF MATERIALS, PART II,
D. Van Nostrand, 1956

REFERENCES (continued)

21. Timoshenko, S. P. and Goodier, J. N.
THEORY OF ELASTICITY, McGraw-Hill, 1951

22. Timoshenko, S. P. and Woinowsky-Krieger, S.
THEORY OF PLATES AND SHELLS, McGraw-Hill, 1959

23. Crandall, S. H.
ENGINEERING ANALYSIS, McGraw-Hill, 1956

24. Richardson, L. F.
THE APPROXIMATE ARITHMETICAL SOLUTION BY FINITE DIFFERENCES OF PHYSICAL PROBLEMS INVOLVING DIFFERENTIAL EQUATIONS, WITH AN APPLICATION TO THE STRESSES IN A MASONRY DAM,
Philosophical Transactions of the Royal Society (London), Series A, Vol. 210, 1910

25. Shaw, F. S.
RELAXATION METHODS, Dover Publications, 1953

26. Hickerson, J. P.
NOTCHED FATIGUE PROPERTIES OF THREE PRESSURE VESSEL STEELS IN LOW-CYCLE FATIGUE,
Master's Thesis, Lehigh University, 1967

ACKNOWLEDGMENTS

The work upon which this report is based was a part of the research conducted on two projects, Fatigue Strength of Welded Plate Girders and Welded Plate Girders - Design Recommendations. Both projects were carried out at Fritz Engineering Laboratory, Department of Civil Engineering, Lehigh University. Doctor Lynn S. Beedle is Director of the Laboratory and Acting Chairman of the Civil Engineering Department.

The projects were sponsored by the Pennsylvania Department of Highways, the U. S. Department of Transportation-Bureau of Public Roads, the American Iron and Steel Institute, the American Institute of Steel Construction, and the Welding Research Council. Both projects were guided by the Welded Plate Girder Committee of the Welding Research Council. The continued support of the sponsors and the assistance of the committee members are gratefully acknowledged.

Appreciation must also be extended to the authors' colleagues for their advice and assistance. The help of Juin S. Huang and Heriberto A. Izquirdo in the handling of computer programs is acknowledged. Thanks are also due to Richard N. Sopko and his staff for preparing the drawings and Mrs. Dorothy Fielding for typing the manuscript.

LEHIGH UNIVERSITY
Bethlehem, Pennsylvania
Department of Civil Engineering
Fritz Engineering Laboratory

327 August 10, 1967

To: Members of the Welded Plate Girder Project Subcommittee

Messrs:

M. Deuterman, Chairman	T. R. Higgins	W. Munse
J. H. Adams	C. D. Jensen	E. Paulet
A. Amirikian	K. Jensen	E. Pisetzner
L. S. Beedle	B. Johnston	E. Ruble
J. Durkee	R. Ketter	J. Vasta
G. Fox	M. Koehler	I. Viest
J. Gilligan	K. Koopman	G. Winter
L. Grover	W. McLean	C. Zwissler

Gentlemen:

At the last Subcommittee Meeting on July 25, an oral presentation was made on girder web boundary stresses and their correlation with fatigue cracks. It was mentioned that a written report would be submitted to the Subcommittee with a ballot. Enclosed is this report, entitled "Girder Web Boundary Stresses and Fatigue" (F.L. Report No. 327.2) and a postcard for the ballot.

In the report the membrane (in-plane) stresses of girder webs are discussed briefly to show that these stresses alone do not account for the fatigue cracks. A method is then described by which web bending stresses (out-of-plane bending stresses) can be estimated quite accurately from measured web deflections. Subsequently, correlation is shown between the web plate bending stresses and the results of fatigue tests. Both the location and the sequence of crack formation are explained by these stresses. The relationship between stresses and fatigue life can be expressed in the form of an S-N curve typical of all fatigue investigations.

As was suggested by the Task Group in the Subcommittee Meeting, minor revisions will be incorporated into the report before submitting it to WRC for publication as a Bulletin. The revisions will include clarification of terminology, addition of available fatigue data obtained after the report was written and, possibly, addition of a table on stress comparison. We expect to complete the revision in about two months and then submit the revised report to the Task Group for further review before publication.

Your comments on the report and your approval of the publication scheme as described will be greatly appreciated.

Sincerely yours,

B. T. Yen
Project Director

BTY:dsk